

School of Physics & Astronomy
Queen Mary University of London

Using Cosmic Void Abundance as a Probe of Dynamical Dark Energy

Samuel F. Kumagai (190562946)

Supervised by Dr Tessa Baker

Submitted September 2020 in part fulfilment of the requirements for the degree of
Master in Astrophysics at Queen Mary University of London

Declaration

I hereby certify that this Dissertation, which is approximately eight thousand words in length, has been written by me at the School of Physics and Astronomy, Queen Mary University of London, that all material in this dissertation which is not my own work has been properly acknowledged, and that it has not been submitted in any previous application for a higher degree.

The sections which contain the report on the independent research work component of the project are Sections [3](#) and [4](#).

Samuel F. Kumagai (190562946)

Acknowledgements

Firstly, I would like to deeply thank Dr Tessa Baker for her expertise, advice, editing, and support that she has provided throughout this entire process.

I would also like to thank a group of teachers and professors for their guidance and mentorship, without which, I would not be in this position: Dr Martha Haynes, Dr Michael Niemack, Charity Smith, and Holly McBroom. I would especially like to thank the late John Threlkeld, for pushing me to do the best I can.

Also, I want to thank my peers in the MSc program for help with everything from formatting to tricky ValueErrors even when I was across the Atlantic for half the year.

I would also like to thank Jake Carnavalla for his programming expertise and general knowledge, and finally my parents for letting me move back in just when they were certain they were rid of me.

Abstract

More than two decades after the discoveries that confirmed the expansion of the universe is accelerating, we still are investigating whether it arises from a constant Λ -term or a mildly varying dynamical dark energy. This research explores whether any signatures of the dark energy equation of state can be found in the evolution of cosmic voids or their size distribution. To do so, we follow Birkhoff's theorem, which means underdense regions evolve as bubble universes with effective cosmological parameters $H_v(t)$, $\Omega_{v,M}(t)$, and $\Omega_{v,\Lambda}(t)$ that depend on the underdensity of the void. We also derive the parameters that govern its evolution using the popular Chevallier-Polarski-Linder parametrization of the dark energy equation of state. We then explore how these parameters affect both models. This result is applied to create a void size distribution that matches theory and observations.

Contents

List of Figures	vi
List of Tables	ix
1 Introduction	1
1.1 Cosmic Depressions	1
1.1.1 Finding Voids	2
1.1.2 Voids in LSS and Cosmology	5
1.2 Expansion of the Universe	6
1.3 Λ CDM and Basic Spacetime Geometry	8
1.3.1 Problems with Λ	10
2 A Theoretical Model of a Cosmic Void	12
2.1 A Void as a Hubble Bubble	12
3 Dynamical Dark Energy	19
3.1 EoS Parametrization	19
4 Analysis and Comparison with ΛCDM	26
4.1 Limits of the Λ CDM Model for the Void	26
4.2 Problems with the CPL Model of a Cosmic Void	28
4.3 Exploring the Void Size Distribution	32
5 Conclusion	36
Bibliography	38

List of Figures

1.1	A slice of thickness $5 \text{ h}^{-1} \text{ Mpc}$ from the center of the region from the Millennium simulation (Springel et al. 2005). Uppermost left panel displays the dark matter distribution and the blue dots are void galaxies. ZOBOV algorithm output is bottom center. <i>Figure from: Colberg et al. (2008)</i>	4
1.2	The cosmic web in an N-body simulation at $z = 1.4$. Matter is pressed between voids to form filaments and walls. <i>Figure from: Springel et al. (2005)</i>	6
1.3	The evolution of different components of energy density in the universe. The matter energy density is extremely close to the cosmological constant energy density at present, otherwise known as the cosmic coincidence problem. <i>Figure from: Debono and Smoot (2016)</i>	11
2.1	Spherical model for the evolution of a cosmic void. Left: a pure top-hat parametrization up to the epoch of shell-crossing. Shell-crossing is when initially interior shells of matter overtake exterior shells in a void. Right: a void with the same characteristics as the top-hat void but angularly averaged. This figure displays the tendency of voids to evolve towards a top-hat like configuration by emptying out its interior. <i>Figure from: van de Weygaert and Platen (2011)</i>	13
2.2	Evolution of $\eta(t)$ when $\eta_f = -25$. This displays how the behavior of $\Omega_\Lambda(t)$ suits the need for a function of time that moderately deviates from the background expansion.	16
2.3	Evolution of the scale factor and void scale factor in a $\delta_v(t_0) = -0.94$ and $\eta_f = -350$ void. We are assuming a background cosmology with $h = 0.7$, $\Omega_{M,0} = 0.3$, and $\Omega_{\Lambda,0} = 0.7$.	18
3.1	Evolution of the CPL EoS with respect to redshift with $w_0 = -0.9, -1.1$ and $w_a = -0.2, -0.4$. These are values that fall within the observational constraints.	20

3.2	Limits on w_0 and w_a from Planck TT+lowP+BAO+JLA data. Contours correspond to 68% and 95% limits. Dashed lines show cosmological constant scenario. <i>Figure from: Planck Collaboration et al. (2016)</i>	21
3.3	Percent difference between the void scale factors solved for from equations (3.12) and (3.13). In this case, $w_0 = -1.1$ and $w_a = 0.3$. Clearly the difference is negligible over all times and the simpler version (3.13) will be used.	23
3.4	Time evolution of the scale factor and void scale factor. We again assume $\Omega_{\Lambda,0} = 0.7$, $\Omega_{M,0} = 0.3$, $h = 0.7$, and we take $\eta_f = -10$. The CPL void scale factor is much more sensitive to $\eta(t)$. This plot has $w_0 = -0.9$, $w_a = -0.09$, both of which are within the limits set by Planck Collaboration et al. (2016).	24
3.5	Time evolution of the energy densities of the background cosmology and void. This plot uses the same parameters as Figure 3.4. Background components are the dashed lines.	25
4.1	An example of the void-in-cloud process from a numerical simulation in an SCDM cosmology ($\Omega_0 = 1.0$, $h = 0.5$). The time evolution of an initially underdense region is shown from the top left panel to the bottom right panel with $a = 0.3, 0.4, 0.5$, and 1.0 , respectively. The void no longer exists at present epoch due to the local overdensities crushing it. <i>Figure from Sheth and van de Weygaert (2004)</i>	27
4.2	Evolution of the scale factor in Λ CDM and in the CPL parametrization. $\eta_f = -50$, $w_0 = -0.7$ and $w_a = 0.09$.	28
4.3	Behavior of CPL and Λ CDM α value with respect to final $\eta(t)$ value, η_f .	29
4.4	Color map of w_0 and w_a with the color representing the value of the CPL void α at that position in the parameter space. In this plot, we have chosen $\eta_f = -25$.	30
4.5	The dependence of α on w_a . $\eta_f = -25$ and the time of void divergence was chosen to be 1 Gy.	30
4.6	CPL model of a void with $\eta_f = -2.5$, $w_0 = -0.7$, $w_a = 0.09$, and $t_{div} = 5$ Gy.	31
4.7	CPL model of a void with $\eta_f = -2.5$, $w_0 = -0.7$, $w_a = 0.09$, and $t_{div} = 11$ Gy.	31

4.8	The dependence of α on t_{div} , or, the time at which the underdense region diverges from the background cosmology. $\eta_f = -25$ in this plot.	31
4.9	Distribution of void radii for four different combinations of w_0 , w_a values. 2000 voids with randomly distributed t_{div} , $\delta_v(t_i)$, and $r_v(t_i)$ were evolved forward until present-epoch.	33
4.10	Distributions of void radii for $w_0 = -1.1$, $w_a = -0.2$. 2000 voids with randomly distributed initial parameters were evolved forward until a chosen cutoff time, at which the value of $a_v(t_{cutoff})$ was used instead of the void's α , which assumes evolution until present time. Clearly, there is a characteristic void scale or peak at a given epoch. Cutoff times are given in Gy.	34
4.11	Mean and median R_{eff} for 250 voids of varying cutoff time in a cosmology with $w_0 = -1.1$, $w_a = -0.2$	35
4.12	Void radius distributions from the Cosmic Void Catalogue of Sutter et al. (2012) . Right panel only includes voids with zero central density. <i>Figure from Pycke and Russell (2016)</i>	35

List of Tables

4.1 Properties of the void size distributions shown in Figure 4.9.	33
--	----

1 Introduction

Cosmology, the study of the origin and evolution of the universe, has developed dramatically in the past half-century. In the early 1980s, the theory of inflation provided a solution to several of cosmology’s thorniest problems and an explanation for the large-scale structure (LSS) that we see in the universe. The cosmic microwave background (CMB) was measured precisely for the first time by the Cosmic Background Explorer satellite, which established the CMB as thermal as well as determining its temperature to an unprecedented level of precision for a cosmological observation ([Mather et al. 1994](#)). However, one of the most drastic paradigm shifts for cosmology came in the late 1990s, as two teams studied standard candles to make distance estimates, in this case, Type Ia supernovae. These supernovae occur when a white dwarf in a binary pair becomes more massive than the Chandrasekhar limit, setting off an explosion with a characteristic luminosity that can then be used for empirical distance estimates ([Sandage and Tammann 1982](#)). Using this result, the teams found that the expansion of the universe was in fact accelerating and therefore space is filled with some sort of dark energy that comprises the majority of the energy density of the universe ([Perlmutter et al. 1999; Riess et al. 1998](#)). The exact mathematical form and physicality behind dark energy is still an active area of study. In this research, we will seek to learn more about dark energy using an often overlooked component of the universe, the vast deserts known as cosmic voids. Specifically, this dissertation will seek to find if the distribution of void sizes is a useful probe of the dark energy equation of state.

1.1 Cosmic Depressions

Cosmic voids formed out of underdensities in the primordial fluctuation field. The prediction of initially negative density perturbations forming cosmic voids was an important result for the CDM model ([Hausman et al. 1983](#)). Work on LSS and cosmology in general has largely focused on the sheets and filaments that make up the cosmic web, clusters, and galaxies, namely the “stuff” that populates space.

However, there is much to be gained from studying areas with little to no matter. There is not yet a unique and universally used definition of a cosmic void, but we do know the principal properties of these objects now. These enormous underdensities formed from negative density perturbations in the primordial universe. Voids are enormous volumes of space with nearly no galaxies in their interior, typically with radii in the range of $20\text{--}50 \text{ h}^{-1} \text{ Mpc}$ ([van de Weygaert and Platen 2011](#)). However, voids can span a wide range of sizes, from “minivoids” that have a radius of a few Mpc ([Tikhonov and Karachentsev 2006](#)), to gigantic “supervoids” that can be as big as a hundred Mpc ([Szapudi et al. 2014](#)). Voids also constitute the dominant volume fraction of the universe ($\approx 95\%$). Only relatively recently have galaxy surveys become large enough to perform statistically significant analyses of voids.

1.1.1 Finding Voids

A significant obstacle for studying voids is due to the lack of a solid definition of what a void actually is. Therefore, in simulations and in real data, void finding algorithms with widely varying criteria are used to identify and classify voids. This makes it very complicated to compare two sets of voids found in different studies. There are three main types of void finders: density-based finders, finders with dynamical criteria, and geometrical algorithms.

The density criterion assumes voids are regions empty of galaxies or with densities lower than a chosen fraction of the mean background density (see [Hoyle and Vogeley \(2002\)](#), [Micheletti et al. \(2014\)](#), [El-Ad and Piran \(1997\)](#), etc.). Typically galaxies are chosen as tracer particles, designated either as field tracers or wall tracers. Field tracers exist in somewhat underdense environments, while wall tracers reside in high-density areas. Cosmic voids are usually taken to contain zero wall tracers in this scenario. The downside of this category of void finders is that a density contrast and the difference between wall and field tracers must be hand-picked, which introduces bias into the criteria of what constitutes a cosmic void.

Dynamical finders rely on a different notion of what defines a cosmic void (see [Lavaux and Wandelt \(2010\)](#), [Elyiv et al. \(2015\)](#), etc.). While density and geometric finders analyze the density of space, dynamical finders define voids as regions where matter streams out from the center. The definition of a void center is likewise different, as in this case, it is the point where particles escape the fastest. These algorithms rely on analyzing gravitationally unstable points in the density field using galaxies as tracers.

The last type of void finders is the geometrical approach. These algorithms iden-

tify voids as geometrical structures in the matter distribution traced by galaxies, such as polyhedra, spheres, or other shapes (see [Sutter et al. \(2015\)](#), [Platen et al. \(2007\)](#), [Shandarin et al. \(2006\)](#), etc.). Several of these methods rely on Voronoi tessellation, which identifies the set of points closer to a center point than to any other center point. After weighing each of these zones against the overall background number or mass density, the algorithm applies the watershed transform to delineate void zones. The watershed transform works by raising the “water level” from local density minima until two zones meet at a density ridge, where a “dam” is constructed. Then, the water level is raised so the entire density landscape is immersed save for the dams. The definition of these cells is parameter-free except for one density threshold under which the dams disappear and the zones merge. This is typically set to the average void underdensity $\delta = -0.8$. [Neyrinck \(2008\)](#) was one of the earliest works to make use of this type of algorithm. This paper introduced the ZOBOV (ZOnes Bordering on Voidness) algorithm which was based on the dark matter halo finder VOBOZ (VOronoi Bound Zones), except instead of looking for local density maxima, ZOBOV looks for minima ([Neyrinck et al. 2005](#)). Due to its parameter-free nature, it became fairly widely used and many subsequent void finders can be considered modifications to ZOBOV’s recipe, such as VIDE (Void IDentification and Examination toolkit) ([Sutter et al. 2015](#)) and the finder proposed and used on SDSS (Sloan Digital Sky Survey) data by [Nadathur and Hotchkiss \(2014\)](#). Additionally, ZOBOV is useful because it also returns the hierarchy of voids, with parent voids and their subvoids sorted accordingly.

Each of these three methods of finding or defining voids has drawbacks and advantages. We can see this in Figure 1.1, which displays the wide differences in the voids returned by different void finding algorithms. ZOBOV-type algorithms typically either have zero parameters or only have one parameter that must be set, but also can return a large number of low-significance voids that come from Poisson noise if not carried out carefully. Dynamical finders have the advantage of using the Lagrangian displacement field, which is still mostly in the linear regime even at $z = 0$ and particularly for voids. This allows users to make nearly exact analytical computations of the dynamics and geometry of cosmic voids ([Lavaux and Wandelt 2010](#)). However, by using the dynamical definition of a void, that a void is a region in which matter is escaping, the ability to compare to other void sets found by the other methods is lost or at the very least is complicated. Additionally, all three methods have to use galaxies as tracers of the overall matter distribution, which is not an exact relation and involves bias prescriptions which are not yet completely understood.

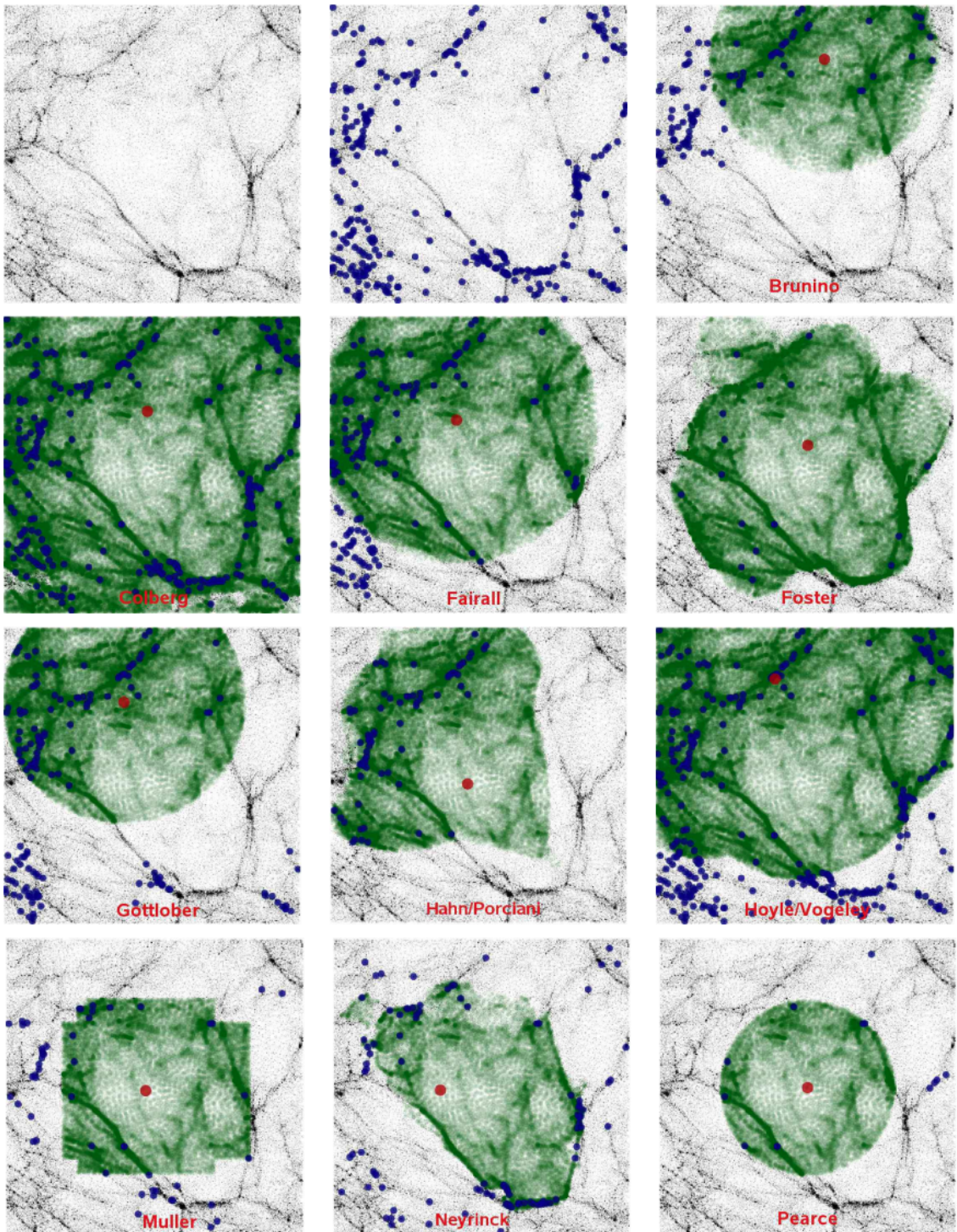


Figure 1.1: A slice of thickness $5 \text{ h}^{-1} \text{ Mpc}$ from the center of the region from the Millennium simulation (Springel et al. 2005). Uppermost left panel displays the dark matter distribution and the blue dots are void galaxies. ZOBOV algorithm output is bottom center.
Figure from: Colberg et al. (2008)

There have been several efforts to systematically compare void finding algorithms. [Colberg et al. \(2008\)](#) used thirteen different void finders on a mock galaxy catalogue from the Millennium Simulation ([Springel et al. 2005](#)) at $z = 0$. This work was not done to rank or decide the best void finders, but rather to comprehend the differences in the algorithms and sets of voids that they return. There were stark differences, such as one finder ([Brunino et al. 2007](#)) found three voids in the volume while another ([Platen et al. 2007](#)) detected 167. Additionally, the radius of the largest cosmic void found varies wildly, from $10 \text{ h}^{-1} \text{ Mpc}$ ([Plionis and Basilakos 2002](#)) to $29.9 \text{ h}^{-1} \text{ Mpc}$ ([Colberg et al. 2005](#)), which is of particular interest to this work since we will be analyzing the void size distribution.

1.1.2 Voids in LSS and Cosmology

Cosmic voids reside in between the walls and filaments of the cosmic web, or perhaps more accurately, the cosmic web exists between the voids. In fact, [Sheth and van de Weygaert \(2004\)](#) propose a model of structure formation that does not track the evolution of virialized haloes, but rather how matter is squeezed in between expanding voids and sheets and filaments form at the intersections of void walls. This model explains the foam-like pattern of the cosmic web better than the work which assumes virialized objects form from smooth spherical collapse. This excursion set analysis of cosmic voids relies on the fact that voids are, on average, spherical and tend towards a spherical top-hat geometry as they grow, which underpins one of our initial assumptions in this paper ([Icke 1984](#)).

Additionally, voids encode a considerable amount of cosmological information since they are relatively untouched and unaffected by later dynamics. Voids are the ideal laboratories for studying cosmological signals such as the integrated Sachs-Wolfe (ISW) effect, the Alcock-Paczynski (AP) test, and analyses of neutrinos can use voids as well ([Kreisch et al. 2019; Lavaux and Wandelt 2012](#)). The ISW signal describes how photons emitted at early times lose energy due to late-time accelerating expansion of the universe degrading gravitational potentials, causing photons to gain energy when traveling through massive structures, and lose energy when traversing a void. Likewise, the AP test essentially compares the physical size of a structure to its angular size. If you have a collection of objects you knew to be spherical on average, such as voids, you can then extrapolate the expansion history of the universe directly. Additionally, voids are ideal locales to test theories of modified gravity (e.g., [Clifton et al. \(2012\)](#)), study baryonic acoustic oscillations (BAO) (e.g., [Kitaura et al. \(2016\)](#)), and voids can also be helpful for astrophysical

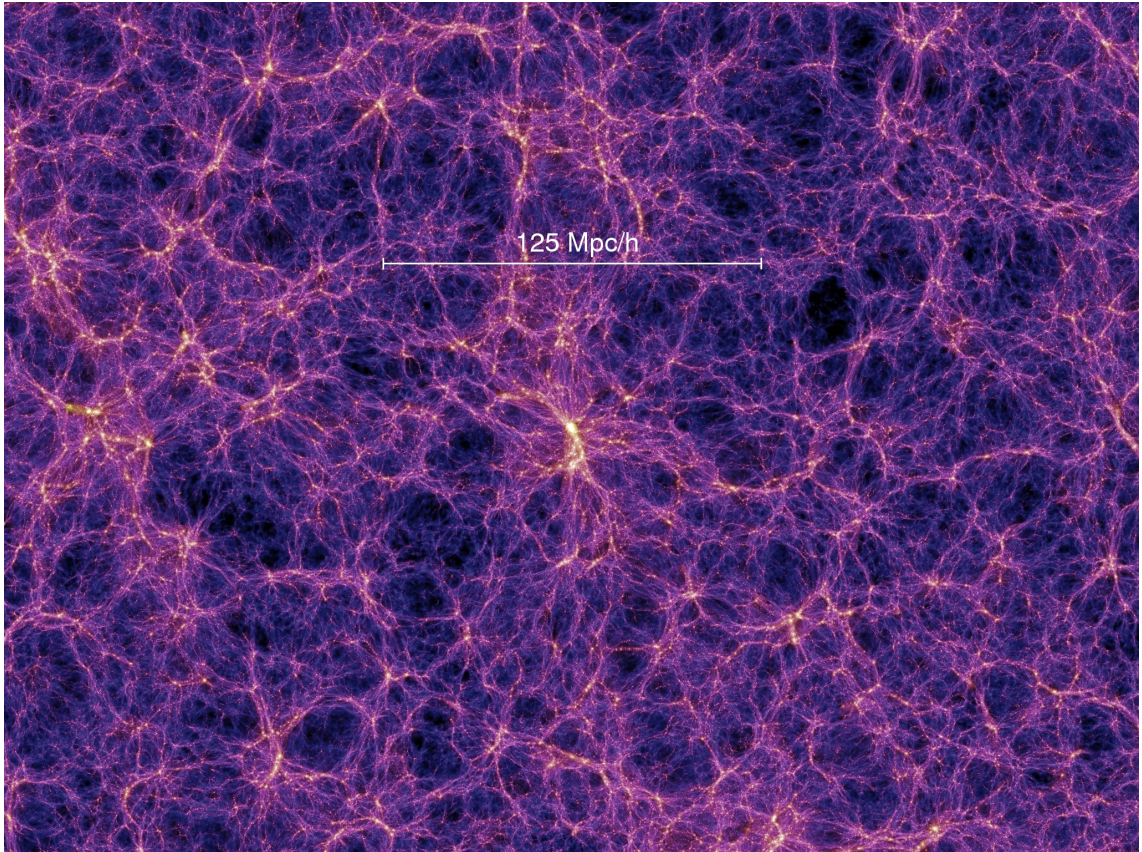


Figure 1.2: The cosmic web in an N-body simulation at $z = 1.4$. Matter is pressed between voids to form filaments and walls. *Figure from: Springel et al. (2005)*

applications, such as studying isolated galaxies in their centers (e.g., Penny et al. (2015)).

While these tests and analyses tie into our own analysis, the aspect of cosmology that this paper will investigate specifically is the dark energy equation of state (EoS). Voids are an excellent place to do this since dark energy dominates the energy budget within voids much earlier than in any other structure. This means that the low matter energy density condition that we now observe in the universe has affected voids for much longer, making them ideal laboratories to look for the effects of dark energy.

1.2 Expansion of the Universe

The expansion of the universe was first discovered when it was found that, in all directions, distant galaxies are receding from us. This discovery was made possible by a phenomenon called redshift. Redshift is when light has an increased wavelength

from either relative motion, the expansion of spacetime itself, or from a strong gravitational field. Although the redshift of other galaxies, or nebulae as they were known in the early 20th century, were observed as early as 1918 by [Slipher \(1918\)](#), the true understanding of the importance of this discovery was not possible until 1929.

At first, it was only possible to calculate the relative distances to the nebulae, using measurements of the angular radius or observed luminosity. Without knowing the absolute luminosity or physical dimensions, many astronomers hypothesized that these nebulae were distant parts of our own galaxy. This all changed in 1929 when Edwin Hubble observed Cepheid variable stars in the Andromeda nebulae (M31). Cepheid variables are bright stars with a characteristic time dependence of their luminosities, a fact discovered by Henrietta Leavitt while studying Cepheid variables in the Small Magellanic Cloud ([Leavitt and Pickering 1912](#)). Cepheids then became the first important extragalactic “standard candle”. Hubble’s discovery of Cepheids in M31 along with Leavitt’s work on the period-luminosity relationship allowed Hubble to measure the distance to M31 and conclude that it was so distant and large it must be its own galaxy. He expanded this analysis to several galaxies with recessional velocities $\approx 1000 \text{ km s}^{-1}$ and found a roughly linear relationship between distance and redshift ([Hubble 1929](#)). Slipher and others did not find this linear relation earlier due to confusion around peculiar velocities, the motions of a galaxy induced by matter in its local neighborhood, which make it difficult to differentiate this motion from pure Hubble flow. The relation that Hubble uncovered can be expressed as

$$v = Hd, \quad (1.1)$$

where v is a galaxy’s recessional velocity, d is the distance to the galaxy, and H is the Hubble constant. The Hubble constant is actually the present value of the Hubble parameter, which quantifies the expansion rate of the universe. We can also now define the cosmological redshift or the stretching of the wavelength of light due to the expansion of space itself. The wavelength shift is related to the redshift z by

$$\frac{\lambda_{obs} - \lambda_{em}}{\lambda_{em}} = z, \quad (1.2)$$

if λ_{obs} is the observed wavelength of light, and λ_{em} is the wavelength of emission. Now that we have defined the cosmological redshift, we can define a parameter

central to much of cosmology and our analysis in particular, the scale factor:

$$a = a(t) = \frac{1}{1+z}. \quad (1.3)$$

The Hubble parameter can be expressed in terms of the scale factor as

$$H = \frac{\dot{a}(t)}{a(t)}. \quad (1.4)$$

However, equation (1.3) is not the source of the scale factor. To find where the scale factor comes from, we must more rigorously define the mathematical framework we will use to describe the universe.

1.3 Λ CDM and Basic Spacetime Geometry

In recent decades, work in cosmology has converged on a standard model, known as the Lambda cold dark matter model (Λ CDM). Λ CDM solves many problems facing cosmologists. It gives an explanation for the structure found in the CMB (Spergel et al. 2003), the aforementioned acceleration of the universe's expansion, the relative abundance of light elements, and the LSS we see today (Cole et al. 2005). Central to the Λ CDM paradigm is the homogeneity and isotropy of the universe and that general relativity (GR) is the correct model of gravitational interactions. Essentially, homogeneity means that the universe would look the same after a coordinate translation, and isotropy implies the same except after a coordinate rotation. Looking up at the night sky, we can say that these assumptions are not true. However, for cosmological purposes, we only care if these assumptions are true on large scales. These crucial assumptions hold until down to around 10 Mpc (Peebles and Ratra 2003). Λ CDM seems to agree with reality quite well and has been tested to a high degree of precision. Confirming or refuting the model remains the most active area of research in cosmology.

To describe our universe quantitatively, we must define the geometry of an isotropic, homogeneous, and three-dimensional space using a metric tensor $g_{ij}(\vec{x})$, where i and j run over the three spatial dimensions. The invariant interval between two arbitrarily close events in some coordinate space is referred to as the line element. We can define the line element as $ds^2 \equiv g_{ij}dx^i dx^j$. The most general line element for

an isotropic and homogeneous space in three dimensions can be expressed as

$$ds^2 = a^2 \left[\frac{dr^2}{1 - kr^2} + r^2 d\Omega^2 \right], \quad d\Omega^2 = d\theta^2 + \sin^2 \theta d\phi^2, \quad k = 0, \pm 1. \quad (1.5)$$

As is standard, the angles θ and ϕ are the azimuthal and polar angles of spherical coordinates, where $\theta \in [0, \pi]$, $\phi \in [0, 2\pi]$. The parameter k describes the curvature of the space: $k = 0$ corresponds to a flat, Euclidean geometry, $k = -1$ is the hyperspherical case, and $k = 1$ is the spherical case. Here the parameter a is simply a dimensionless variable.

We can expand the description of this space to four dimensions by changing from Latin indices that span the three spatial coordinates to Greek indices that include time as well: $ds^2 = g_{\mu\nu} dx^\mu dx^\nu$, or $ds^2 = -dt^2 + a(t)^2 d\vec{x}^2$. Then we can define the Friedmann-Robertson-Walker (FRW) metric as

$$g_{\mu\nu} dx^\mu dx^\nu = ds^2 = -dt^2 + a(t)^2 \left[\frac{dr^2}{1 - kr^2} + r^2(d\theta^2 + \sin^2 \theta d\phi^2) \right], \quad (1.6)$$

where $a(t)$ is still dimensionless, but is now a function of time that parametrizes the relative expansion of the universe. Note that in this equation, and throughout the remainder of this work we shall be using units where the speed of light is unity. There is a theorem that says this form of the metric is the unique solution (up to a coordinate transformation) if the universe seems spherically symmetric and isotropic to a set of freely falling observers, see [Weinberg \(1972\)](#), chapter 13.5.

In Λ CDM, the expansion of the universe is governed by Einstein's field equations (EE), which can be expressed as

$$G_{\mu\nu} + \Lambda g_{\mu\nu} = 8\pi G T_{\mu\nu}, \quad (1.7)$$

where $G_{\mu\nu}$ is the Einstein tensor, Λ is the cosmological constant, G is the gravitational constant, and $T_{\mu\nu}$ is the stress-energy tensor. Λ is defined as $\Lambda = 8\pi G \rho_\Lambda$ where ρ_Λ is the vacuum energy density. The cosmological constant was originally inserted into the field equation by Einstein in order for the equations to describe a static universe, the paradigm at the time ([Einstein 1917](#)). However, this cosmology was highly unstable. When the expansion of the universe became widely accepted, Einstein called the cosmological constant his greatest mistake. Ironically, calling it a mistake was truly the mistake since we now have great reason to expect a non-vanishing vacuum energy.

For a spatially flat FRW metric ($k = 0$), the solutions for EE's go from a non-linear

system of ten partial differential equations to two ordinary non-linear differential equations:

$$H(t)^2 = \left[\frac{\dot{a}(t)}{a(t)} \right]^2 = \frac{8\pi G}{3}\rho + \frac{\Lambda}{3}, \quad (1.8)$$

$$\frac{\ddot{a}(t)}{a(t)} = -\frac{4\pi G}{3}(\rho + 3p) + \frac{\Lambda}{3}, \quad (1.9)$$

where a dot indicates a derivative with respect to global time, and p and ρ are the proper pressure and energy density, which contains contributions from matter, dark matter, and radiation. These are the Friedmann equations that constrain the FRW universe. By combining these two equations, we can obtain the conservation law

$$\dot{\rho} = -3\frac{\dot{a}}{a}(\rho + p). \quad (1.10)$$

In Λ CDM, we assume that the EoS for the pressure has the form $p = w\rho$, where w is the EoS parameter. Now that we have p as a function of ρ , we can solve equation (1.10) to find ρ as a function of time:

$$\rho(t) \propto a^{-3(1+w)}. \quad (1.11)$$

There is a different EoS parameter for each type of fluid that contributes to the overall ρ , namely $\{w_\Lambda, w_m, w_r\} = \{-1, 0, \frac{1}{3}\}$ with the ws corresponding to dark energy, matter, and radiation respectively.

1.3.1 Problems with Λ

While using a cosmological constant with an EoS $w = -1$ parametrizes the universe we see well, it is by no means perfect. To begin with, we do not have an understanding of the physical process or processes that underlie dark energy. Quantum field theory (QFT) posits that the zero-point energy of the vacuum contributes to the cosmological constant. QFT predicts a vacuum energy density around $(300 \text{ GeV})^4$ or 10^{27} g/cm^3 , which differs from the observed value of about 10^{-29} g/cm^3 by a staggering 56 orders of magnitude. There are many theorized contributions and cancellations that will hypothetically span this vast difference, but any cancellation would have to be accurate to 56 decimal places as well (Weinberg 2008).

There are many theories that can parametrize aspects of dark energy, such as supersymmetry or string theory, but these theories can often introduce even more complications. Additionally, while Λ CDM assumes an EoS of $w = -1$ and this parametrization is consistent with observational data, see [Planck Collaboration et al.](#)

(2018), there is no fundamental reason why ρ_Λ should be constant in every epoch of the universe's history.

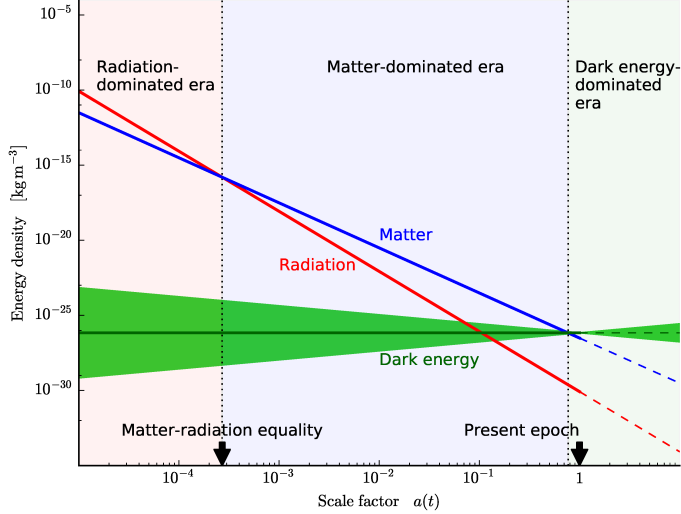


Figure 1.3: The evolution of different components of energy density in the universe. The matter energy density is extremely close to the cosmological constant energy density at present, otherwise known as the cosmic coincidence problem. *Figure from: Debono and Smoot (2016)*

Another problem with our current understanding of dark energy is that its energy density at the present epoch is comparable to the matter energy density, which has been termed the cosmic coincidence problem. These fundamental issues with our understanding of the nature of Λ , along with the so-called H_0 (Riess et al. 2016) and σ_8 (Basilakos and Nesseris 2017) tensions, present significant theoretical and observational discrepancies within Λ CDM. Clearly, new approaches and perhaps even new physics are necessary to bridge the divide.

2 A Theoretical Model of a Cosmic Void

So far, we have established that cosmic voids are objects of importance and utility to both cosmology and astrophysics, particularly for learning more about the nature of dark energy. In practice, much of the study of voids is done through simulations. Some of this has to do with the difficulty associated with acquiring enough data points from extremely sparse areas of the universe. Additionally, survey masks and boundaries can wreak havoc on void distributions and number counts. In theory, simulating voids ought to be much easier than other patches of the cosmic web, since voids have intrinsically simpler dynamics. However, if we are looking at void regions in a typical numerical simulation run, only $\approx 6\%-8\%$ of the mass and a fraction of the volume of the simulation is in the areas that we are interested in. This is extremely computationally expensive, particularly if numerous cosmological models need to be run. In this section, we will discuss a potential solution to this problem from [Goldberg and Vogeley \(2004\)](#) that also gives us a useful way to explore the physics in a void.

2.1 A Void as a Hubble Bubble

We know that voids remain in the linear regime for a longer time and evolve towards sphericity over the course of their existence. These are two key assumptions in how we will approximate the evolution of a void. We approximate a cosmic void as an expanding and isolated universe unto itself. Isolated we take to mean there is no accretion of mass from other regions of the universe at large. Since voids are by nature underdense, they create an effectively repulsive peculiar gravitational influence. This means that initially underdense areas expand quicker than the Hubble flow.

The key to this analysis is Birkhoff's theorem, which tells us that the internal dynamics of a spherical system are unaffected by objects or dynamics in the exterior universe ([Birkhoff and Langer 1923](#)). The condition of voids evolving towards a

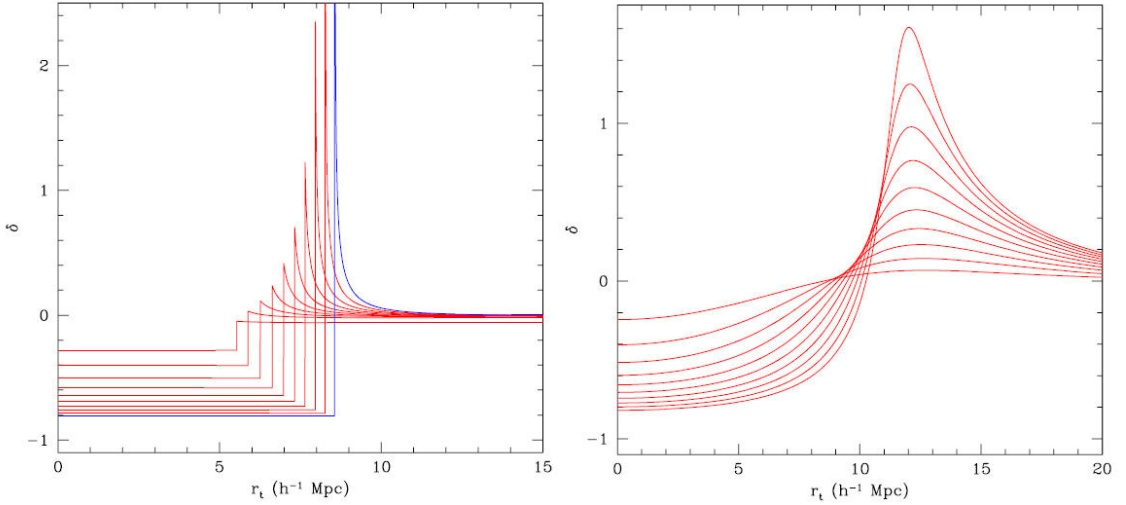


Figure 2.1: Spherical model for the evolution of a cosmic void. Left: a pure top-hat parametrization up to the epoch of shell-crossing. Shell-crossing is when initially interior shells of matter overtake exterior shells in a void. Right: a void with the same characteristics as the top-hat void but angularly averaged. This figure displays the tendency of voids to evolve towards a top-hat like configuration by emptying out its interior. *Figure from: van de Weygaert and Platen (2011)*

spherical top-hat configuration, as shown in Figure 2.1, allows us to apply this to a hypothetical cosmic void. Therefore, a spherically symmetric region with a given mean density, cosmological constant density, radius r , and expansion rate \dot{r} will evolve exactly as a universe with Hubble parameter \dot{r}/r and mean density equal to that of the region. In this section, we are still working within Λ CDM, and therefore assume a matter density from CDM and baryons of ρ_0 at present time and neglect the density of relativistic matter. The full derivation can be found in [Goldberg and Vogeley \(2004\)](#) but we will cover the essentials for clarity.

All subscripts of “0” refer to a quantity measured at present time, and the subscript “v” will refer to any property of the void region itself. At an arbitrarily high redshift, the scale factor is $a_i = a(t_i) = 1/(1 + z_i)$. We consider a spherical region that is underdense with a radius $r_v(t_i)$. This region is embedded in a background cosmology with CDM and baryon matter density of ρ_0 at present. If we define the density contrast of the void as $\delta_v(t_i)$, then the mass inside the spherical region is

$$M_v = \frac{4\pi}{3} r_v(t)^3 [1 + \delta_v(t)] \frac{\rho_0}{a(t)^3}, \quad (2.1)$$

which is conserved at all times. We also define a dimensionless variable

$$a_v(t) = a_i \frac{r_v(t)}{r_v(t_i)}, \quad (2.2)$$

from which we see that at very early times $a_v(t) = a(t)$. By differentiating equation (2.1) with respect to time and using equation (2.2) we find

$$\frac{\dot{r}_v(t)}{r_v(t)} - \frac{\dot{a}(t)}{a(t)} + \frac{\dot{\delta}_v}{3(1 + \delta_v(t))} = 0. \quad (2.3)$$

Since the void is spherically symmetric and Birkhoff's theorem applies, we can write a Friedmann equation that describes its evolution as a “Hubble Bubble” in the flat background cosmology as

$$\left[\frac{\dot{r}_v(t)}{r_v(t)} \right]^2 = \frac{8\pi G \rho_v(t)}{3} + \frac{\Lambda_v}{3} - \frac{k_v}{R_v(t)^2}, \quad (2.4)$$

where $R_v(t)$ is the radius of curvature inside the void, and k_v is the sign of its curvature. In this section we will proceed with a Λ_v equal to that of the background universe, so the subscript is dropped from here forward. From equation (2.1) we can see that $\rho_v(t) = [1 + \delta_v(t)] \frac{\rho_0}{a(t)^3}$, and expand the right-hand side of equation (2.4) as

$$\begin{aligned} \frac{8\pi G \rho_v(t)}{3} + \frac{\Lambda_v}{3} - \frac{k_v}{R_v(t)^2} &= H_0^2 \frac{\Omega_{M,0}}{a^3} + H_0^2 \Omega_{\Lambda,0} + \delta_v(t) H_0^2 \frac{\Omega_{M,0}}{a^3} - \frac{k_v}{R_v(t)^2} \\ &= \left(\frac{\dot{a}}{a} \right)^2 + \delta_v(t) H_0^2 \frac{\Omega_{M,0}}{a^3} - \frac{k_v}{R_v(t)^2}, \end{aligned} \quad (2.5)$$

where we have substituted $(\dot{a}/a)^2$ for the first two terms as the Friedmann equation of the flat background cosmology, $\Omega_{M,0} = \frac{8\pi G \rho_0}{3H_0^2}$ is the present value of the matter energy density parameter, and $\Omega_{\Lambda,0} = \frac{\Lambda}{3H_0^2}$ is the present value of the vacuum energy density. Now we can use equation (2.3) to expand the left-hand side of equation (2.4) as

$$\left[\frac{\dot{r}_v(t)}{r_v(t)} \right]^2 = \left(\frac{\dot{a}}{a} \right)^2 \left[1 - \frac{a \dot{\delta}_v(t)}{3 \dot{a} [1 + \delta_v(t)]} \right]^2 \quad (2.6)$$

If $\delta_v \propto a$, then $\dot{\delta}_v \propto \dot{a}$, and we assume $|\delta_v| \ll 1$, then equation (2.6) can be rewritten

as

$$\begin{aligned}
&= \left(\frac{\dot{a}}{a} \right)^2 \left[1 - \frac{\delta_v(t)}{3} (1 + \delta_v(t))^{-1} \right]^2 \\
&\simeq \left(\frac{\dot{a}}{a} \right)^2 \left[1 - \frac{\delta_v(t)}{3} (1 - \delta_v(t)) \right]^2 \\
\left[\frac{\dot{r}_v(t)}{r_v(t)} \right]^2 &\simeq \left(\frac{\dot{a}}{a} \right)^2 \left[1 - \frac{2\delta_v(t)}{3} \right].
\end{aligned} \tag{2.7}$$

All equations before equation (2.7) were fully general, however, the final two equalities in equation (2.7) only hold at the early times in the evolution of the void, since that is when $\delta_v \propto a$ and $|\delta_v| \ll 1$.

We can now combine equations (2.5) and (2.7) to get the following relation that applies to early times only

$$-\frac{2\delta_v(t)}{3} \left(\frac{\dot{a}}{a} \right)^2 = \delta_v(t) H_0^2 \frac{\Omega_{M,0}}{a^3} - \frac{k_v}{R_v(t)^2}. \tag{2.8}$$

If we substitute the background Friedmann equation $H^2(t) = H_0^2(\Omega_{M,0}/a^3 + \Omega_{\Lambda,0})$ again, we get

$$\begin{aligned}
\frac{1}{R_v(t)^2} &= -\frac{5}{3}\delta_v(t) H_0^2 \frac{\Omega_{M,0}}{a^3} \\
R_v(t) &= \frac{a}{H_0} \sqrt{\frac{-3a(t)}{5\delta_v(t)\Omega_{M,0}}}.
\end{aligned} \tag{2.9}$$

where we have set $k_v = -1$, as is necessarily the case for an underdense region in a flat cosmology. The $\Omega_{\Lambda,0}$ term has been dropped as it is small compared to the $\Omega_{M,0}/a^3$ term at early times. It is evident that $R_v \propto a_v$ for all times. Therefore, if we look at the case $t \rightarrow 0$, we can say

$$R_v(t) = \frac{a_v(t)}{H_0} \sqrt{\frac{-3a_i}{5\delta_v(t_i)\Omega_{M,0}}}, \tag{2.10}$$

provided that we select t_i early enough. We can now define an important parameter in this model, η . So far in this derivation, we have been following the procedure of [Goldberg and Vogeley \(2004\)](#) fairly closely. They define η as

$$\eta \equiv \frac{\delta_v(t_i)}{a_i}. \tag{2.11}$$

However, since we are looking to model the gradual deviation of the void bubble from the background universe, we shall hereon treat η as a function of time. Specifically we will, somewhat arbitrarily, define $\eta(t)$ as a function of the background vacuum

energy density, $\Omega_\Lambda(t)$. We choose this function as it has a range of $(0, 1)$ that we can tailor the evolution to emulate the gradual breaking off using a parameter that represents the final value of $\eta(t)$ that we want, η_{final} or η_f . Therefore, we can define $\eta(t)$ as

$$\eta(t) = \frac{\eta_f}{\Omega_{\Lambda,0}} \times \Omega_\Lambda(t), \quad (2.12)$$

where $\Omega_{\Lambda,0}$ is the value of $\Omega_\Lambda(t)$ at present day, which we take to be 0.7. Note that η is negative over its entire domain, as we expect from the [Goldberg and Vogeley \(2004\)](#) definition of η in equation (2.11), since $\delta_v(t_i)$ is necessarily negative.

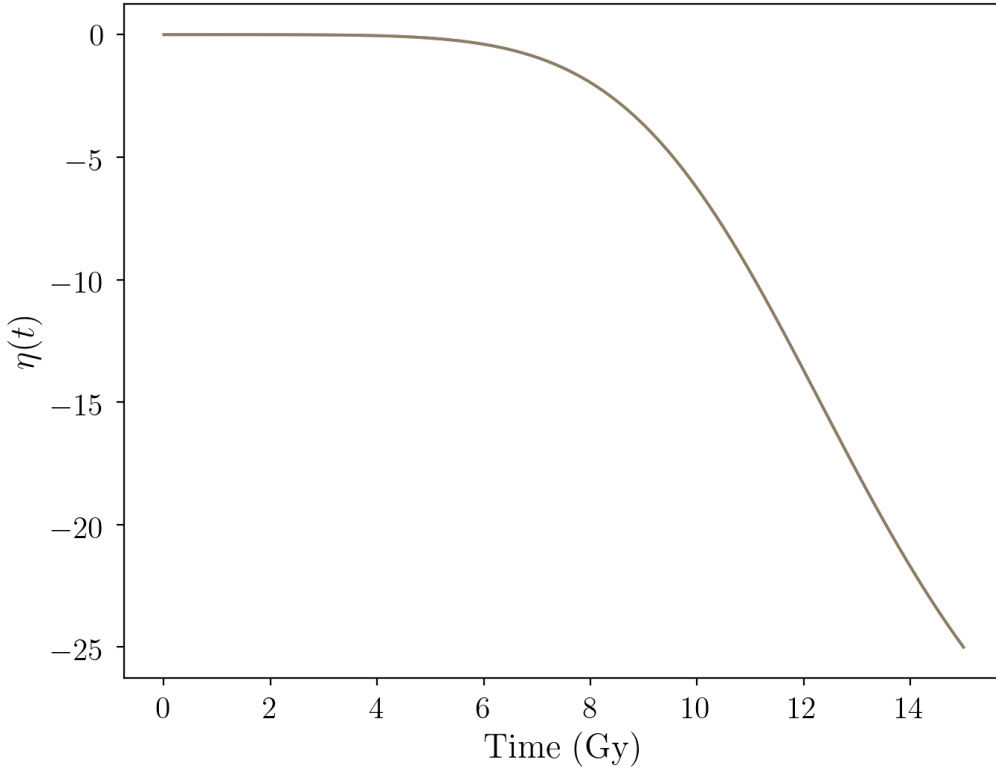


Figure 2.2: Evolution of $\eta(t)$ when $\eta_f = -25$. This displays how the behavior of $\Omega_\Lambda(t)$ suits the need for a function of time that moderately deviates from the background expansion.

Having defined η , we can now write the complete Friedmann equation for the void as

$$\begin{aligned} H_v^2(t) &= \left[\frac{\dot{a}_v(t)}{a_v(t)} \right]^2 = \frac{8\pi G \rho_v(t)}{3} + \frac{\Lambda}{3} - \frac{k_v}{R_v(t)^2} \\ H_v^2(t) &= \frac{H_0^2 \Omega_{M,0}}{a_v^3} + H_0^2 \Omega_{\Lambda,0} - H_0^2 \frac{5\eta(t)\Omega_{M,0}}{3a_v^2}, \end{aligned} \quad (2.13)$$

where we retain the subscripts “0” to signify a parameter’s value at present time for clarity.

We can then define explicit functions for the energy density of matter, vacuum, and curvature in the void, such that $\Omega_M(t) + \Omega_\Lambda(t) + \Omega_k(t) = 1$ for all times:

$$\Omega_M(t) = \frac{H_0^2 \Omega_{M,0}}{H_v^2(t) a_v^3}, \quad \Omega_\Lambda(t) = \frac{H_0^2 \Omega_{\Lambda,0}}{H_v^2(t)}, \quad \Omega_k(t) = -\frac{5\eta(t)\Omega_{M,0}H_0^2}{3a_v^2 H_v^2(t)}. \quad (2.14)$$

If we call $\alpha \equiv a_v(t_0)$, we can also define the density contrast at present epoch by

$$\delta_v(t_0) = \frac{1 - \alpha^3}{\alpha^3}. \quad (2.15)$$

We can now integrate equation (2.13) from t_{div} , or the point when the void’s expansion diverges from the background Hubble flow, to t_0 or present epoch. Figure 2.3 displays the result of this integration. As we expect, $\alpha > a(t_0)$, since an underdense region in a flat background cosmology will expand faster than its surroundings. The work done in this section constitutes a mathematical model of a void that approximates it as an expanding, isolated universe unto itself.

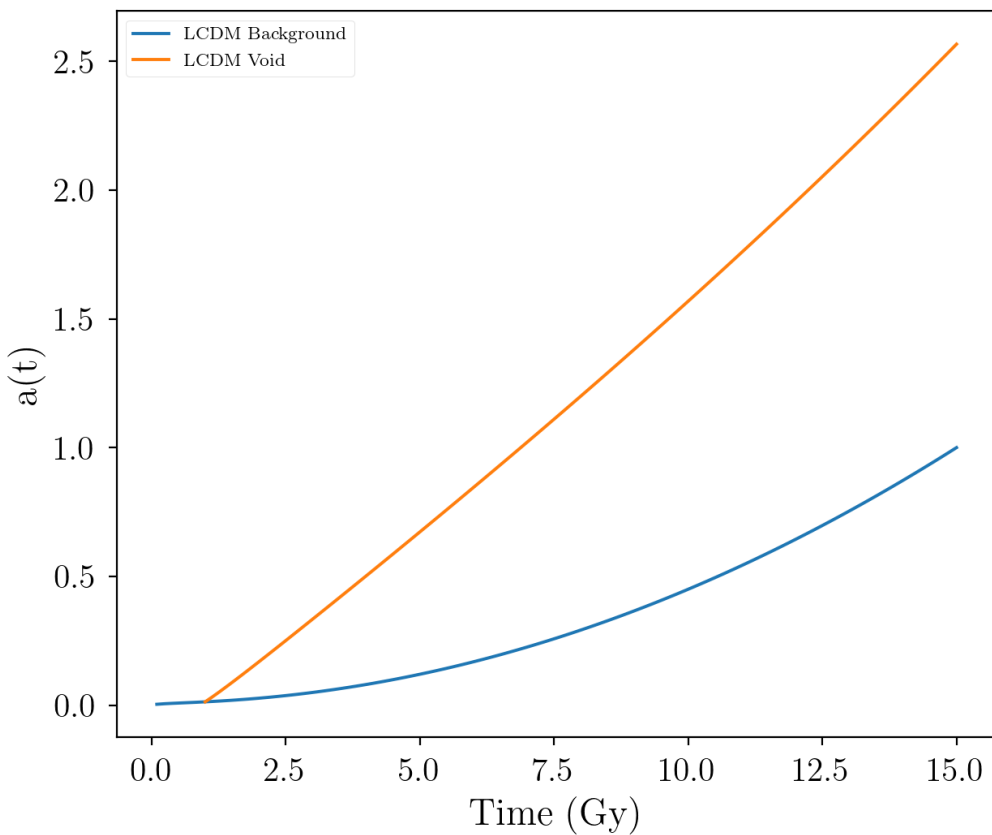


Figure 2.3: Evolution of the scale factor and void scale factor in a $\delta_v(t_0) = -0.94$ and $\eta_f = -350$ void. We are assuming a background cosmology with $h = 0.7$, $\Omega_{M,0} = 0.3$, and $\Omega_{\Lambda,0} = 0.7$.

3 Dynamical Dark Energy

Many theories that reconcile all or some of these incongruities have been proposed. These models often involve theorized time-dependence of the vacuum energy. Quintessence models invoke an evolving scalar field first proposed in [Ratra and Peebles \(1988\)](#). The Chaplygin gas model attempts to unify dark matter and dark energy. Its pressure $p \sim -1/\rho$ gives a solution that behaves as nonrelativistic matter at early times and like a cosmological constant at late times ([Fabris et al. 2002](#)). Chameleon fields involve the scalar field coupling to the baryon energy density and also allow variation across cosmic scales ([Khoury and Weltman 2004](#)). There are many more models and possibilities, each with their own drawbacks and advantages. To look beyond Λ CDM we must explore cosmologies with $w \neq -1$. These can either be time-dependent or independent, with the former being the most general scenario. The model that we will consider in this section is a very general model that can accommodate many features of different models while remaining simple and easy to work with.

3.1 EoS Parametrization

In this work, we explicitly allow that the EoS w evolves with time. The specific parametrization of the EoS that we will be using is that of [Chevallier and Polarski \(2001\)](#) and [Linder \(2003\)](#), henceforth referred to as the CPL model or parametrization. We assume an EoS for dark energy of form

$$w(a) = w_0 + w_a(1 - a), \quad (3.1)$$

$$w(z) = w_0 + \frac{w_a z}{1 + z}, \quad (3.2)$$

where w_0 , and w_a are constants, and a cosmological constant is recovered in the limit $w_0 \rightarrow -1$ and $w_a \rightarrow 0$. In this parametrization, w_0 and w_a have a natural physical interpretation: w_0 represents the EoS's present value, and w_a represents its overall time evolution.

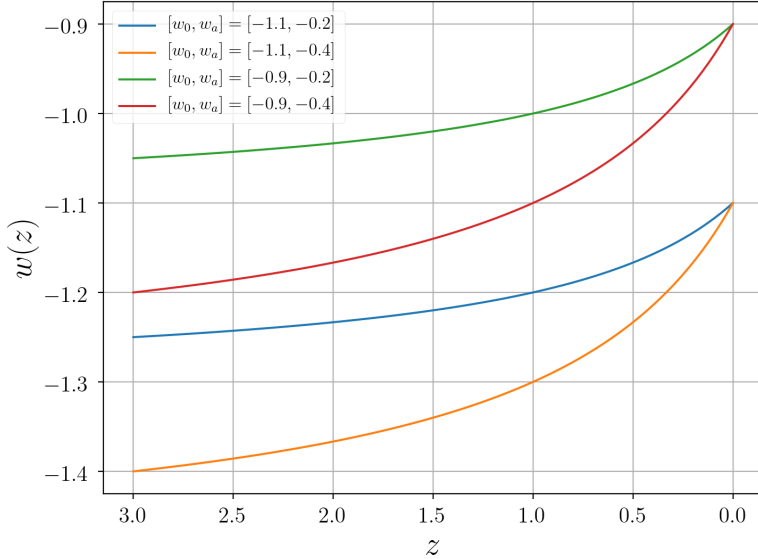


Figure 3.1: Evolution of the CPL EoS with respect to redshift with $w_0 = -0.9, -1.1$ and $w_a = -0.2, -0.4$. These are values that fall within the observational constraints.

This model reduces to linear redshift behavior for low z , is well-behaved at high redshift, which previous models of form $w(z) = w_0 + w_1 z$ failed to capture, has a manageable two-dimensional phase space, and is sensitive to observational data as well. We will be using values of w_0 and w_a within the observational bounds set by [Planck Collaboration et al. \(2016\)](#). This approximately corresponds to $w_0 \in [-1.2, -0.6]$ and $w_a \in [-1.6, 0.8]$.

Having already derived [Goldberg and Vogeley \(2004\)](#)'s model for a theoretical cosmic void in Λ CDM, we will now present the salient steps in deriving the same with the CPL model instead of $w = -1$. Again, if we assume that Birkhoff's theorem applies to the typical cosmic void, then we can specify the evolution of an underdense region. To do so, we assume a specified mean background density with only CDM and baryons of ρ_0 and negligible energy density of relativistic matter.

Up to equation (2.4), the CPL model has no impact. Now that we have a dynamical equation of state however, the second term on the right-hand side of equation (2.4) is dynamical as well, yielding the following relation for the void bubble's Friedmann equation:

$$\left[\frac{\dot{r}_v(t)}{r_v(t)} \right]^2 = \frac{8\pi G \rho_v(t)}{3} + \frac{8\pi G \rho_\Lambda(t)}{3} - \frac{k_v}{R_v(t)^2}. \quad (3.3)$$

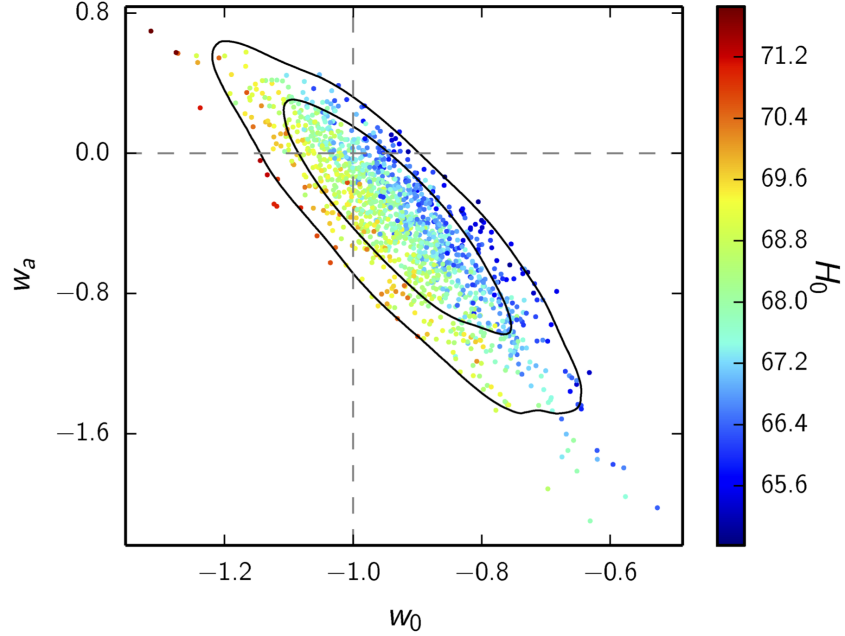


Figure 3.2: Limits on w_0 and w_a from Planck TT+lowP+BAO+JLA data. Contours correspond to 68% and 95% limits. Dashed lines show cosmological constant scenario. *Figure from: Planck Collaboration et al. (2016)*

We can solve for $\rho_\Lambda(t)$ by applying the continuity equation (1.10), which means that

$$\dot{\rho}_\Lambda = -3H(\rho_\Lambda + p_\Lambda), \quad (3.4)$$

where ρ_Λ and p_Λ are the vacuum energy density and proper pressure respectively. From the CPL EoS, equation (3.1), we can rewrite this as

$$\dot{\rho}_\Lambda = -3H\rho_\Lambda(1 + w_0 + w_a(1 - a)). \quad (3.5)$$

If we directly integrate from a general point in time to present epoch, we get the following explicit form of $\rho_\Lambda(t)$:

$$\rho_\Lambda(t) = \rho_{\Lambda 0}a(t)^{-3(1+w_0+w_a)}e^{3w_a(a-1)}, \quad (3.6)$$

where $\rho_{\Lambda 0}$ is the value of the vacuum energy density at present epoch. Using this, we can expand out equation (3.3) as

$$\left[\frac{\dot{r}_v(t)}{r_v(t)} \right]^2 = H_0^2 \frac{\Omega_{M,0}}{a^3} + H_0^2 \Omega_{\Lambda,0} \frac{e^{3w_a(a-1)}}{a^{3(1+w_0+w_a)}} + \delta_v(t) H_0^2 \frac{\Omega_{M,0}}{a^3} - \frac{k_v}{R_v(t)^2}. \quad (3.7)$$

We then substitute (\dot{a}/a) for the first two terms, since we are still assuming a flat background. This yields equation (2.5) exactly. We then follow the steps of [Goldberg and Vogeley \(2004\)](#) up until equation (2.9), where we instead substitute the CPL parametrization form of the flat background Friedmann equation: $H^2(t) = H_0^2 \left(\frac{\Omega_{M,0}}{a^3} + \Omega_{\Lambda,0} \frac{e^{3w_a(a-1)}}{a^{3(1+w_0+w_a)}} \right)$ to get

$$-\frac{2\delta_v(t)}{3} H_0^2 \left[\frac{\Omega_{M,0}}{a^3} + \Omega_{\Lambda,0} \frac{e^{3w_a(a-1)}}{a^{3(1+w_0+w_a)}} \right] = \delta_v(t) H_0^2 \frac{\Omega_{M,0}}{a^3} - \frac{k_v}{R_v(t)^2}. \quad (3.8)$$

This can be simplified further, recalling that an underdense region in a flat cosmology necessarily has $k_v = -1$:

$$\begin{aligned} -\frac{\delta_v(t)}{3} \frac{1}{a^3} H_0^2 \left[5\Omega_{M,0} + 2\Omega_{\Lambda,0} \frac{e^{3w_a(a-1)}}{a^{3(w_0+w_a)}} \right] &= \frac{1}{R_v(t)^2}, \\ R_v(t) &= \frac{a}{H_0} \sqrt{\frac{-3a}{\delta_v(t)}} \left[5\Omega_{M,0} + 2\Omega_{\Lambda,0} \frac{e^{3w_a(a-1)}}{a^{3(w_0+w_a)}} \right]^{-\frac{1}{2}}. \end{aligned} \quad (3.9)$$

As $R_v(t)$ is the radius of curvature inside the void, it is clear that $R_v(t) \propto a_v(t)$ for all times. Therefore, if we take the case as $t \rightarrow 0$, we can say

$$\lim_{t \rightarrow t_i} R_v(t) = \frac{a_v(t)}{H_0} \sqrt{\frac{-3a_i}{\delta_v(t_i)}} \left[5\Omega_{M,0} + 2\Omega_{\Lambda,0} \frac{e^{3w_a(a_i-1)}}{a_i^{3(w_0+w_a)}} \right]^{-\frac{1}{2}}. \quad (3.10)$$

We then similarly to the Λ CDM procedure define $\eta \equiv \frac{\delta_v(t_i)}{a_i}$, and find

$$R_v(t) = \frac{a_v}{H_0} \sqrt{\frac{-3}{\eta}} \left[5\Omega_{M,0} + 2\Omega_{\Lambda,0} \frac{e^{3w_a(a_i-1)}}{a_i^{3(w_0+w_a)}} \right]^{-\frac{1}{2}}. \quad (3.11)$$

We can then write the general form for the Friedmann equation for the void, which is valid for all times:

$$\begin{aligned} H_v^2(t) &= \left[\frac{\dot{a}_v(t)}{a_v(t)} \right]^2 = \frac{8\pi G \rho_v(t)}{3} + \frac{8\pi G \rho_\Lambda(t)}{3} - \frac{k_v}{R_v(t)^2} \\ &= \frac{H_0^2 \Omega_{M,0}}{a_v(t)^3} + H_0^2 \Omega_{\Lambda,0} \frac{e^{3w_a(a_v(t)-1)}}{a_v(t)^{3(1+w_0+w_a)}} - H_0^2 \frac{\eta}{3a_v(t)^2} \left[5\Omega_{M,0} + 2\Omega_{\Lambda,0} \frac{e^{3w_a(a_i-1)}}{a_i^{3(w_0+w_a)}} \right]. \end{aligned} \quad (3.12)$$

However, if we drop the $\Omega_{\Lambda,0}$ term as we did in the Λ CDM derivation, the void

Friedmann equation reduces to

$$H_v^2(t) = \frac{H_0^2 \Omega_{M,0}}{a_v(t)^3} + H_0^2 \Omega_{\Lambda,0} \frac{e^{3w_a(a_v(t)-1)}}{a_v(t)^{3(1+w_0+w_a)}} - H_0^2 \frac{5\eta \Omega_{M,0}}{3a_v(t)^2}. \quad (3.13)$$

The difference between equation (3.12) and equation (3.13) is minuscule at all times, provided that a_i is selected early enough. Figure 3.3 displays how little difference there is between the two differential equations' solutions, with an $a_i = 0.01$.

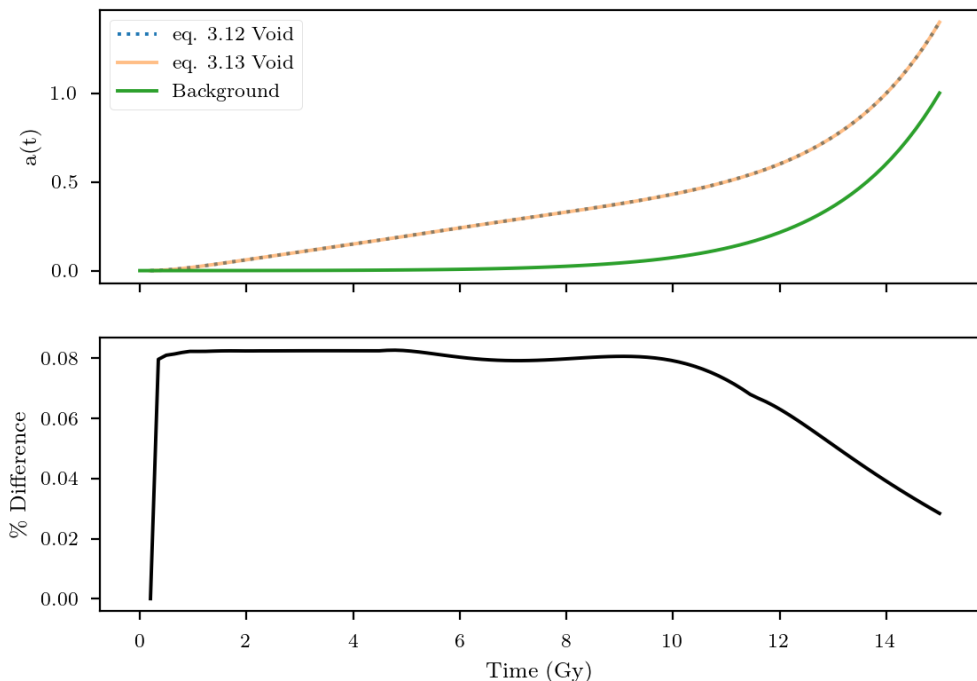


Figure 3.3: Percent difference between the void scale factors solved for from equations (3.12) and (3.13). In this case, $w_0 = -1.1$ and $w_a = 0.3$. Clearly the difference is negligible over all times and the simpler version (3.13) will be used.

We will assume equation (3.13) is a good enough approximation and use that form throughout the remainder of this paper. Now that we have defined the void Friedmann equation in a universe with a CPL parametrization EoS, we can write the explicit functions for the energy densities as well:

$$\Omega_{M,v}(t) = \frac{H_0^2 \Omega_{M,0}}{H_v^2(t) a_v^3}, \quad \Omega_{\Lambda,v}(t) = \frac{H_0^2 \Omega_{\Lambda,0}}{H_v^2(t)} \frac{e^{3w_a(a_v(t)-1)}}{a_v^{3(1+w_0+w_a)}}, \quad \Omega_{k,v}(t) = -\frac{5\eta(t) \Omega_{M,0} H_0^2}{3H_v^2(t) a_v^2}. \quad (3.14)$$

Figure 3.4 displays the evolution of the background and void scale factor in the CPL model of dark energy.

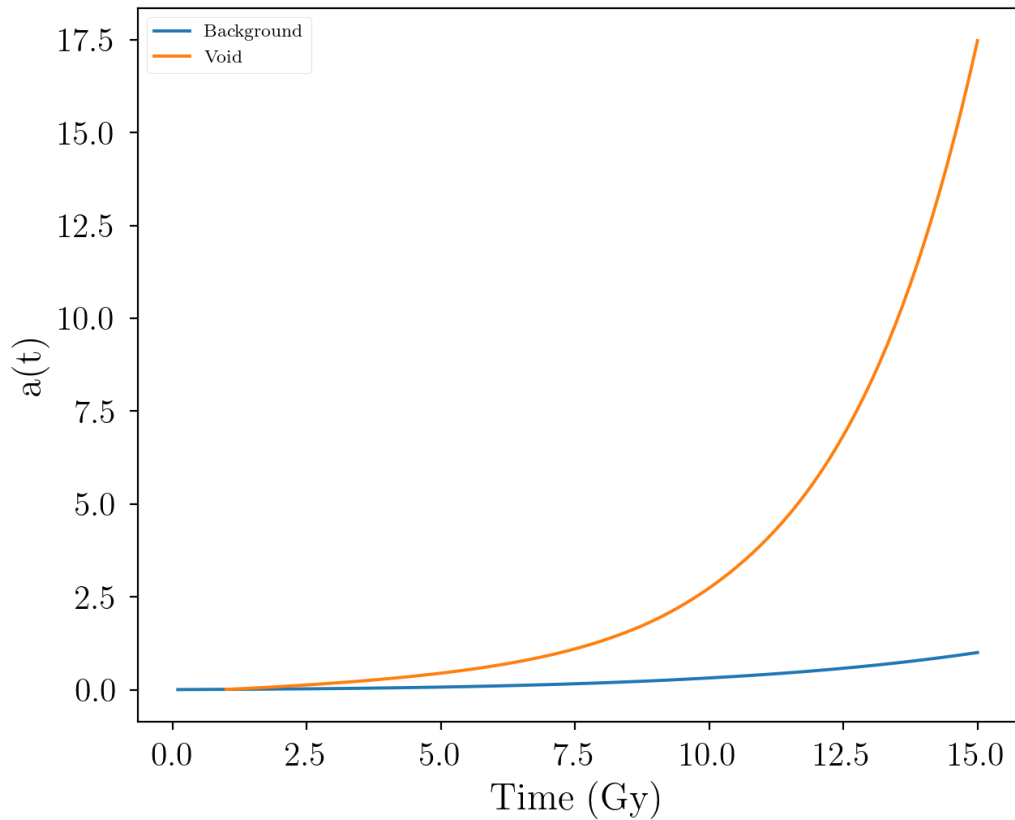


Figure 3.4: Time evolution of the scale factor and void scale factor. We again assume $\Omega_{\Lambda,0} = 0.7$, $\Omega_{M,0} = 0.3$, $h = 0.7$, and we take $\eta_f = -10$. The CPL void scale factor is much more sensitive to $\eta(t)$. This plot has $w_0 = -0.9$, $w_a = -0.09$, both of which are within the limits set by [Planck Collaboration et al. \(2016\)](#).

From Figure 3.5 we can see that the void's vacuum energy density dominates much quicker than in the background cosmology, which helps drive the expansion of the void and results in the void α being greater than one.

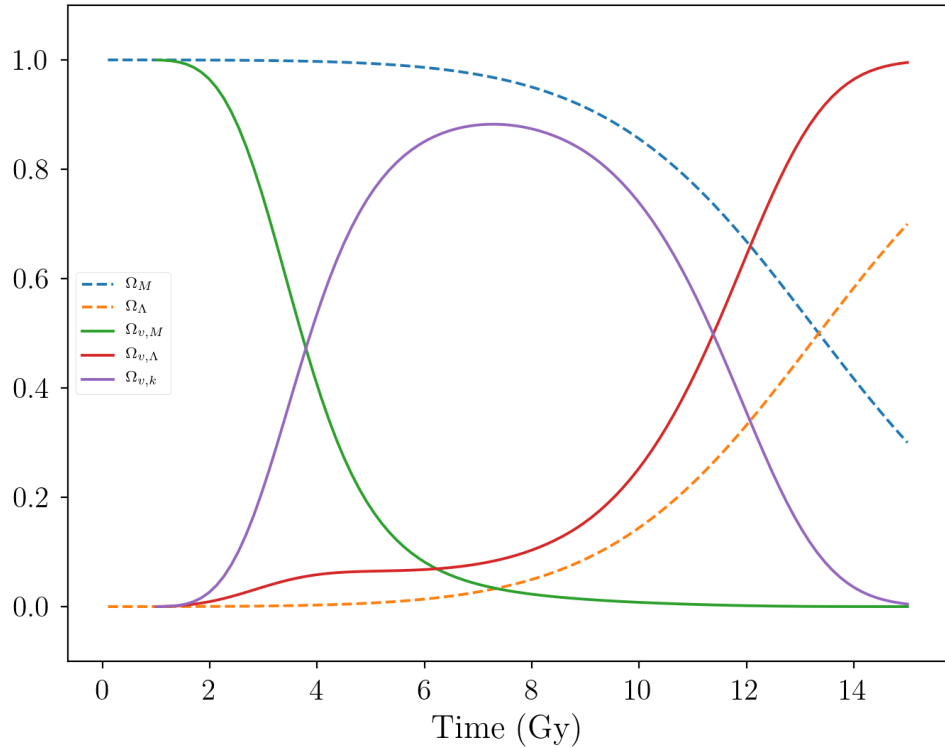


Figure 3.5: Time evolution of the energy densities of the background cosmology and void. This plot uses the same parameters as Figure 3.4. Background components are the dashed lines.

4 Analysis and Comparison with Λ CDM

Now that we have derived a theoretical model of a cosmic void under the Λ CDM and CPL EoS parametrizations, we can compare these results against each other and also apply this result to explore the void size distribution. However, before we can create a model of the size distribution and explore how voids grow throughout cosmic time, we must address the shortcomings of both the Λ CDM and CPL parametrizations of a void.

4.1 Limits of the Λ CDM Model for the Void

This model does an excellent job at analytically describing the evolution of a cosmic void as a miniature universe with negative curvature. The goal of [Goldberg and Vogeley \(2004\)](#) was to create a recipe for simulating voids based off of the derivation that we performed in Chapter 2 as well as the calculation of the primordial power spectrum in the voids. The steps of the recipe broadly are: select the present-epoch underdensity $\delta_v(t_0)$ of the voids that we are interested in, choose the overall background cosmological parameters, compute the effective cosmological parameters in the interior of the underdense region by numerically integrating equation (2.13), and then calculate the initial power spectrum. Once that is done a simulation can be constructed with these parameters, provided that the box length is not a multiple of the void diameter. An advantage of using this approach to study LSS and structure formation is that this method takes the void's effective Hubble constant being larger than the background into account, unlike some excursion set models (e.g. [Sheth and Tormen \(2002\)](#)).

These extra steps for forming a simulation result in a significant increase in speed and efficiency. [Goldberg and Vogeley \(2004\)](#) additionally cite an order of magnitude increase in mass resolution and an increase in spatial resolution as well using these techniques. Therefore, this model is very successful at what it sets out to

do. However, it is less than perfect for more local analyses of voids. Since this model smoothes out structure on the largest scale, it is only valid in the interiors of large voids, as long-range tidal effects break the sphericity and simple dynamics of the model. Additionally, it does not factor in the void compensation walls that we theorize and observe surrounding most voids ([Hamaus et al. 2014](#)). Due to this, analyzing any internal substructure in a cosmic void is impossible with this analysis as well.

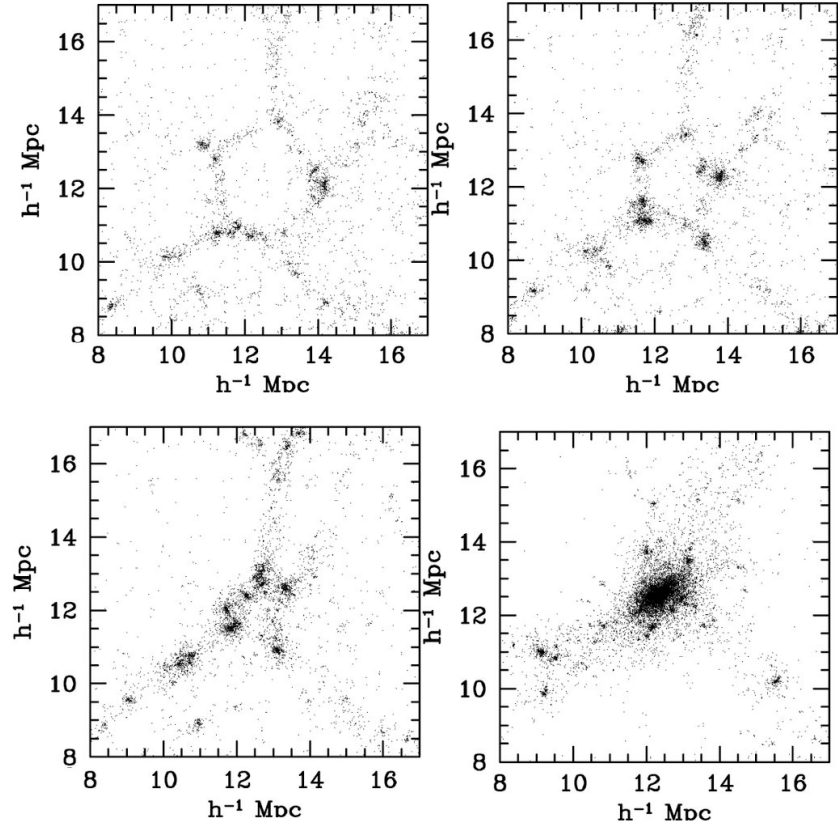


Figure 4.1: An example of the void-in-cloud process from a numerical simulation in an SCDM cosmology ($\Omega_0 = 1.0$, $h = 0.5$). The time evolution of an initially underdense region is shown from the top left panel to the bottom right panel with $a = 0.3, 0.4, 0.5$, and 1.0 , respectively. The void no longer exists at present epoch due to the local overdensities crushing it. *Figure from Sheth and van de Weygaert (2004)*

[Sheth and van de Weygaert \(2004\)](#) state that any complete analysis of structure formation using voids will incorporate both the local matter distribution and also the substructure present within the primordial volume of the void. By treating voids as a collection of spherical and smoothly expanding bubbles, we ignore some of the most crucial aspects in structure formation, that voids have internal structure that affects their evolution, and that there are no isolated voids. Additionally, nowhere in the

analysis is there a possibility of the “void-in-cloud” effect, where a void is crushed out of existence by a surrounding overdensity, that Sheth and van de Weygaert (2004) parametrize well in their double-barrier excursion set approach. However, these shortcomings do not mean this analysis is useless. This analysis allows us to constrain the evolution of an underdense region in a relatively straightforward way that can be used in many different cosmological applications.

4.2 Problems with the CPL Model of a Cosmic Void

We will now consider the results of our derivation in Chapter 3 of the same model as Goldberg and Vogeley (2004) but with the CPL parametrization of the dark energy EoS. While the result in general is aligned with that of the model in Λ CDM, there are some notable differences and odd sensitivities to certain parameters. If we plot both of the solutions for $a_v(t)$ given the same final $\eta(t)$ value, η_f , we can see how the two solutions respond.

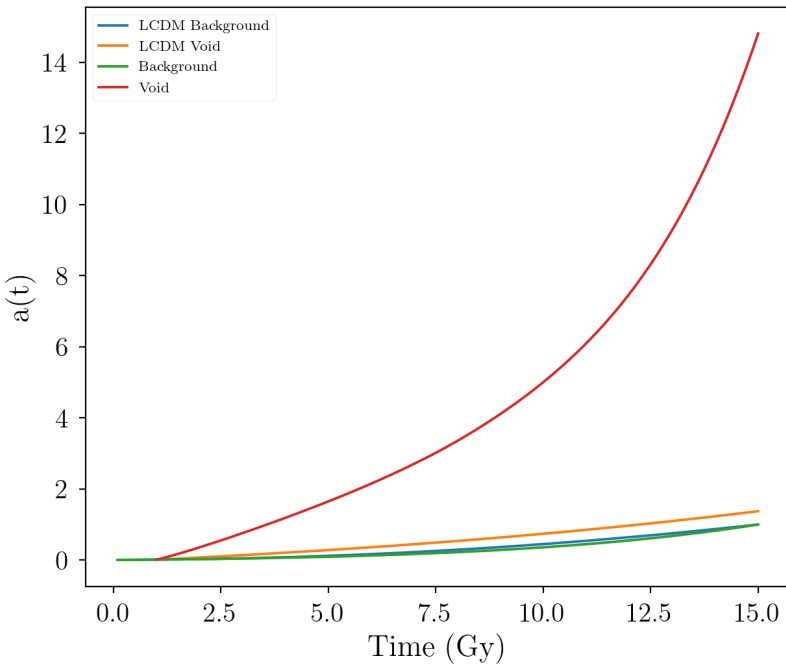


Figure 4.2: Evolution of the scale factor in Λ CDM and in the CPL parametrization. $\eta_f = -50$, $w_0 = -0.7$ and $w_a = 0.09$.

Figure 4.2 displays the scale factor for both the void and the background in the Λ CDM and CPL cases. The CPL parametrization is clearly much more sensitive to $\eta(t)$. We can observe the overall effect of η_f by plotting it against the void's α , or the present-epoch value of the void scale factor numerically integrated for using equations (2.13) and (3.13), respectively.

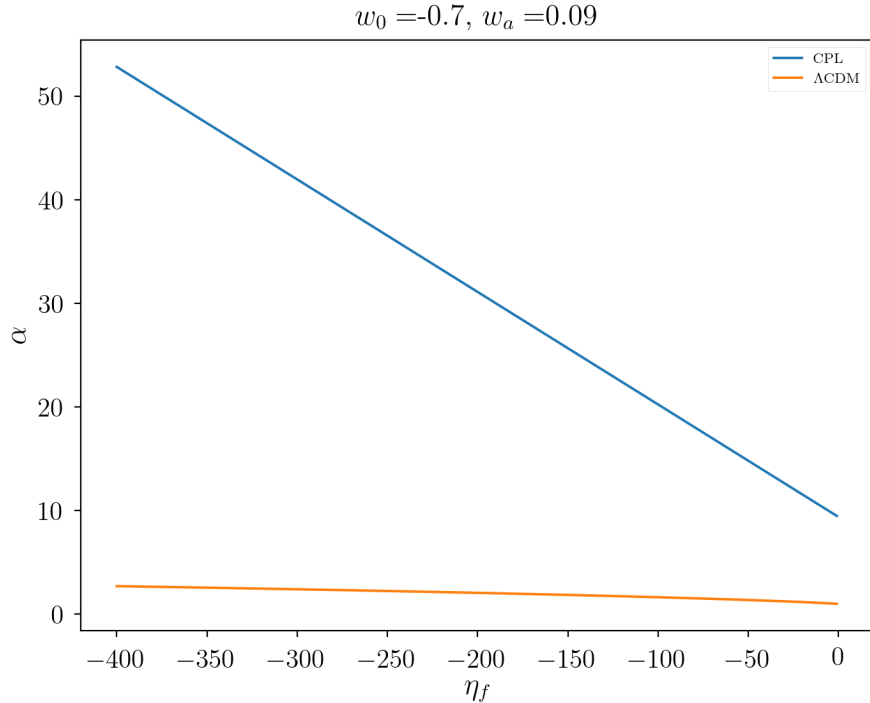


Figure 4.3: Behavior of CPL and Λ CDM α value with respect to final $\eta(t)$ value, η_f .

Even though the $\eta(t)$ for both models are identically defined, and both undergo the same renormalization process, the CPL model responds much more strongly to large values of η_f . This feature of the model itself makes it difficult to compare the two models directly through the evolution of their scale factors. In fact, for different values of w_0 and w_a the degeneracy gets even worse, with CPL model α s reaching as high as 10^7 . Figure 4.4 displays this behavior, assuming the void splits off from the flat background cosmology at $t = 1$ Gy.

Clearly, α is much more strongly affected by w_a . Figure 4.5 again assumes the time of divergence of the void from the background is 1 Gy. As we can see α blows up to values $\approx 10^6$ for $w_a > 0.6$, and even lower values of w_a can result in $\alpha \approx 10^3$, which is still two orders of magnitude higher than what we observe in the Λ CDM formulation.

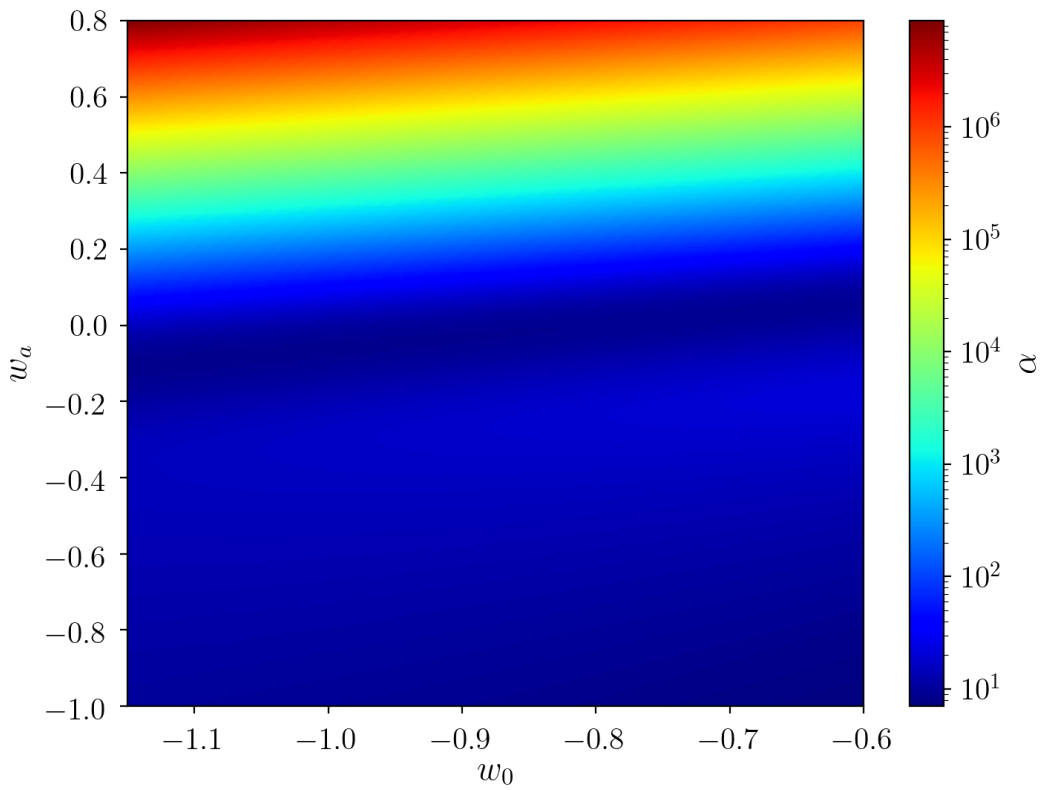


Figure 4.4: Color map of w_0 and w_a with the color representing the value of the CPL void α at that position in the parameter space. In this plot, we have chosen $\eta_f = -25$.

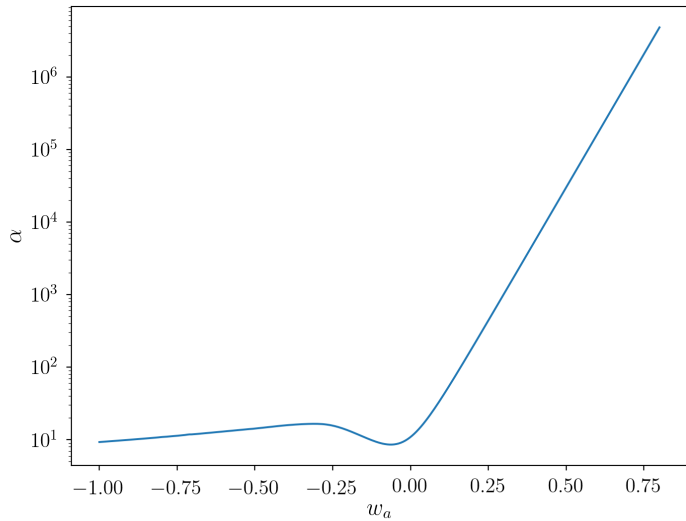


Figure 4.5: The dependence of α on w_a . $\eta_f = -25$ and the time of void divergence was chosen to be 1 Gy.

All of this makes choosing w_a very difficult. However, if we select w_a s that do not lead to enormous α values, we can work with this model of a cosmic void. Fortunately for us, the range in parameter space of w_a delineated in [Planck Collaboration et al. \(2016\)](#) is mostly negative, as it runs from $w_a = -1.6$ to $w_a = 0.8$. As the procedures for solving the respective Friedmann equations and renormalizing the solutions was identical for the Λ CDM and CPL cases, it is odd that η_f affects the CPL model so much more, while the issues with w_a are more expected since w_a can be difficult to constrain in cosmological analyses.

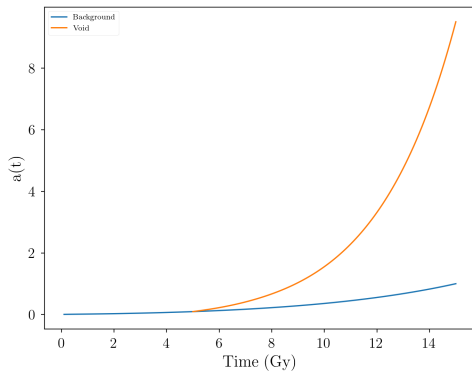


Figure 4.6: CPL model of a void with $\eta_f = -2.5$, $w_0 = -0.7$, $w_a = 0.09$, and $t_{div} = 5$ Gy.

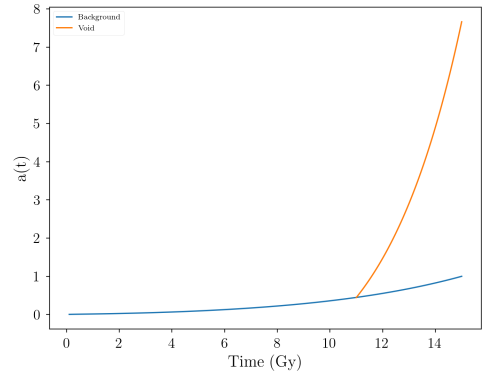


Figure 4.7: CPL model of a void with $\eta_f = -2.5$, $w_0 = -0.7$, $w_a = 0.09$, and $t_{div} = 11$ Gy.

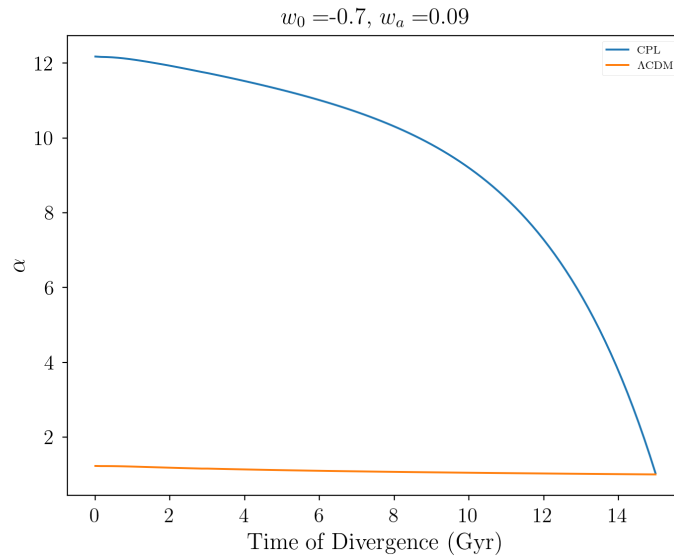


Figure 4.8: The dependence of α on t_{div} , or, the time at which the underdense region diverges from the background cosmology. $\eta_f = -25$ in this plot.

Another parameter in our model that we can explore is the time of divergence from the background cosmology. All of the plots up to this point have had $t_{div} = 1$ Gy. While [Goldberg and Vogeley \(2004\)](#) evolve their voids from the beginning of the universe, we can specify at what time we want the void to begin its evolution, as seen in Figures 4.6 and 4.7. We expect that the later the time of divergence, the smaller the α . This behavior is shown in Figure 4.8.

4.3 Exploring the Void Size Distribution

Now that we have explored the features and shortcomings of our model of a void, we can apply this result to exploring the void size distribution. This was first measured in Λ CDM simulations by [Platen et al. \(2008\)](#) using the watershed transform, which was briefly described in Section 1.1. This work confirmed the prediction of the double-barrier excursion set formalism that [Sheth and van de Weygaert \(2004\)](#) used to model the hierarchical evolution of the overall void population. The double-barrier excursion set had several predictions for the distribution of voids, but the most salient points were that since the void-in-cloud process kills off small voids, there will be a small-scale cutoff in the size distribution and that at a given epoch there is a characteristic void size that evolves with time. As the majority of voids in the universe will have similar sizes to the characteristic scale, the universe at the largest scales will resemble a foam composed of spherical voids of similar size.

While we will not be applying our result to the full Fisher-matrix approach used to study the void size distribution by [Verza et al. \(2019\)](#) and others, we can still put our CPL model of a cosmic void to good use. We randomly distribute void divergence times t_{div} from the beginning of the universe until present-epoch, initial underdensities $\delta_v(t_i)$ from -0.2 to -0.01, and initial void radii $r_v(t_i)$ from 0.9 to $6 \text{ h}^{-1} \text{ Mpc}$. These bounds are somewhat arbitrary, but are reasonable values based off of what we know about void evolution. Then we will integrate the void Friedmann equation for the full evolution of each void given its t_{div} , $\delta_v(t_i)$, and $r_v(t_i)$. Finally, we can solve for the void size at present time, $r_v(t_0)$, using the definition of the void scale factor in equation (2.2), which gives

$$r_v(t_0) = \frac{\alpha r_v(t_i)}{a_i}. \quad (4.1)$$

This analysis will be applied to four different cosmologies with dark energy EoS parameters seen in Figure 3.1, with $w_0 = -1.1, -0.9$ and $w_a = -0.2, -0.4$.

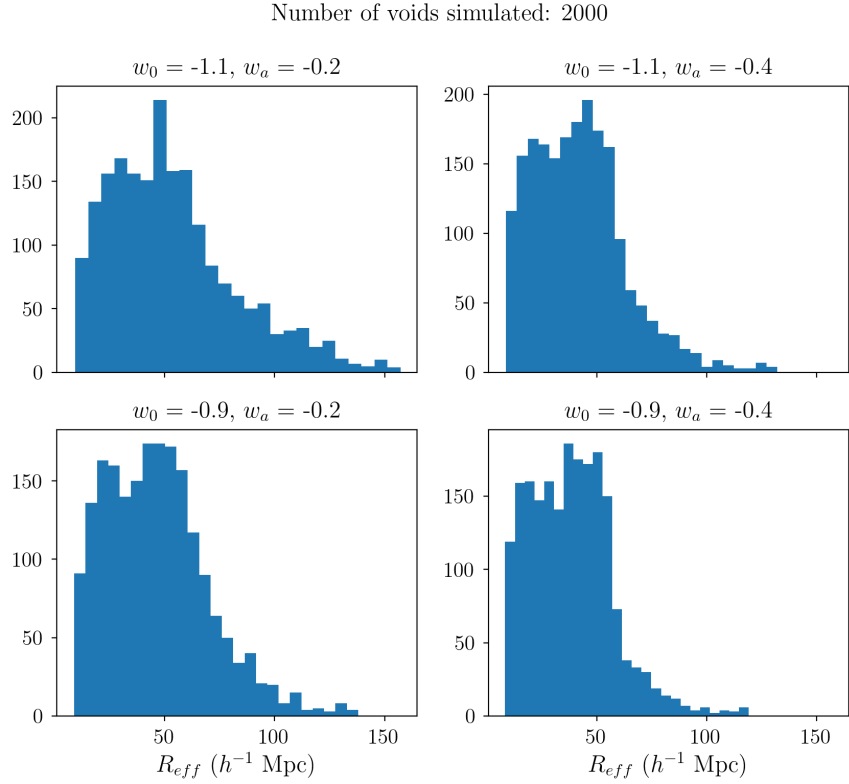


Figure 4.9: Distribution of void radii for four different combinations of w_0 , w_a values. 2000 voids with randomly distributed t_{div} , $\delta_v(t_i)$, and $r_v(t_i)$ were evolved forward until present-epoch.

w_0	w_a	Mean R_{eff} (h^{-1} Mpc)	σ (h^{-1} Mpc)
-1.1	-0.2	53.67	29.14
-1.1	-0.4	41.90	21.22
-0.9	-0.2	46.51	23.40
-0.9	-0.4	38.44	18.74

Table 4.1: Properties of the void size distributions shown in Figure 4.9.

While this process relies on numerous simplifications, it is nonetheless a useful approximation of how voids form throughout cosmic time. Table 4.1 displays the mean and standard deviation for each of the four panels in Figure 4.9. In particular, our simplified model of void formation and evolution features the characteristic void size at a given epoch predicted by Sheth and van de Weygaert (2004). To demonstrate this, the same process that produced Figure 4.9 was used, except an additional parameter was added, the time at which we freeze each void’s evolution and ignore voids that diverged from the flat background after the “cutoff” time. This allows us to approximate what the void size distribution looked like at any

time from the beginning of the universe to $z = 0$. Figure 4.10 displays how this affects the distribution. As expected, voids given more time to evolve continue to expand, especially since none are crushed out of existence by the void-in-cloud effect or other local dynamics slowing or interfering with their expansion.

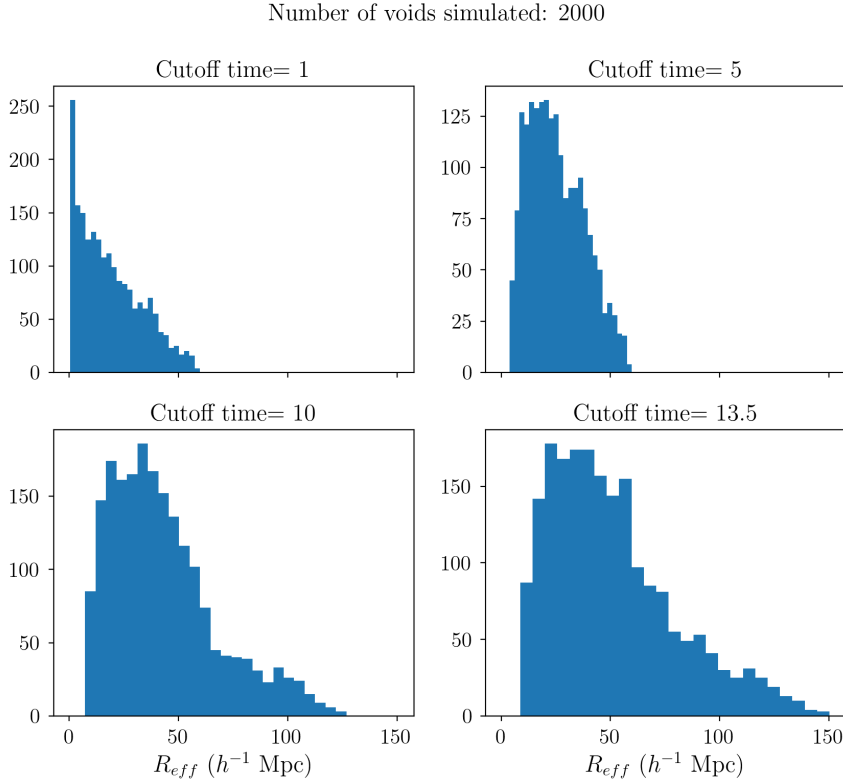


Figure 4.10: Distributions of void radii for $w_0 = -1.1$, $w_a = -0.2$. 2000 voids with randomly distributed initial parameters were evolved forward until a chosen cutoff time, at which the value of $a_v(t_{cutoff})$ was used instead of the void's α , which assumes evolution until present time. Clearly, there is a characteristic void scale or peak at a given epoch. Cutoff times are given in Gy.

Additionally, we can perform this process repeatedly to see how the mean and median void size changes with time. Figure 4.11 displays this relationship.

The mean characteristic void scale grows almost continuously with time, but the median R_{eff} is flat until enough time has gone by for enough voids to grow large enough to increase its value.

So while our CPL model of the evolution of a cosmic void has shortcomings and unforeseen complications within the (w_0, w_a) parameter space that make it difficult to directly compare with the Λ CDM case, it is still a useful model. We can compare our void size distribution with others found in both simulations and observations and find several of the same characteristics and behaviors, for example in Figure

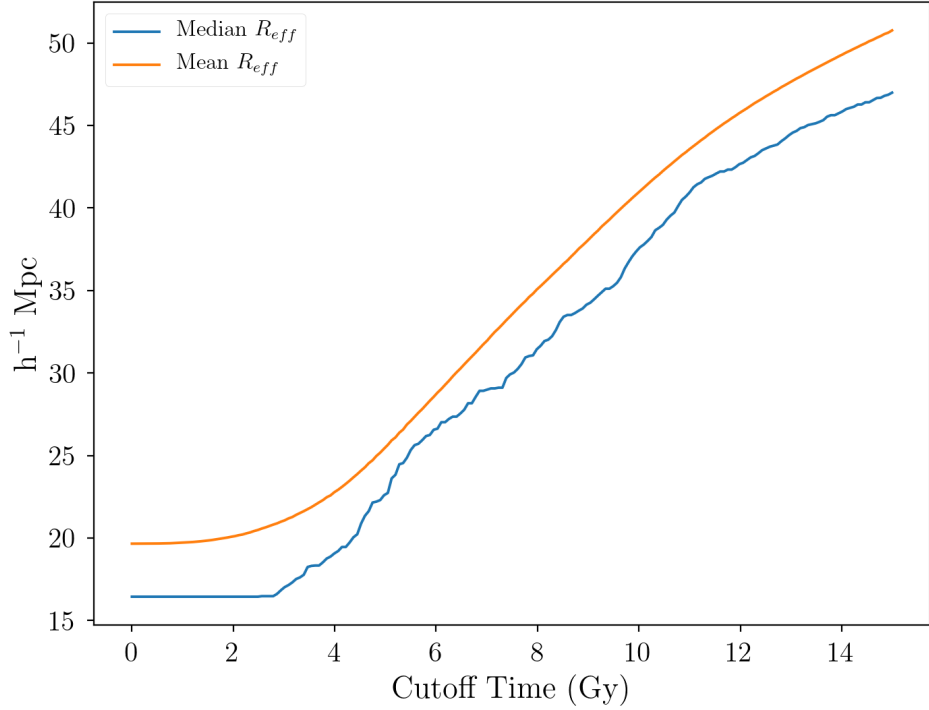


Figure 4.11: Mean and median R_{eff} for 250 voids of varying cutoff time in a cosmology with $w_0 = -1.1$, $w_a = -0.2$.

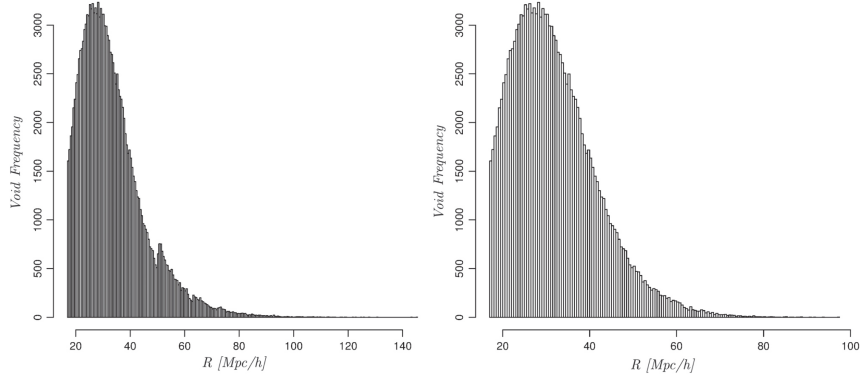


Figure 4.12: Void radius distributions from the Cosmic Void Catalogue of [Sutter et al. \(2012\)](#). Right panel only includes voids with zero central density. *Figure from Pycke and Russell (2016)*

[4.12](#), which shows a void distribution set and subset. Our method overestimates the amount of large voids compared to other works, but the analysis is still valid. Of course, as outlined in Section [1.1.1](#), the definition of a void greatly impacts the radius distribution as well.

5 Conclusion

This Thesis has set out to investigate whether or not the void size distribution is a useful probe of dynamical dark energy. Specifically, we looked at the two-parameter CPL model of time-dependent dark energy EoS. This model has the advantage of having relatively simple dynamics and linear behavior at low redshift. In order to create the void size distribution, it was necessary to formulate a theoretical model of a cosmic void and how it evolves with respect to time. We used [Goldberg and Vogeley \(2004\)](#)'s procedure with the CPL EoS to derive a void Friedmann equation, since an underdense region in a flat cosmology behaves as its own “bubble” universe with a negative curvature and higher effective Hubble parameter than the background. However, we made adjustments to the Λ CDM derivation, specifically altering the η parameter, as we wanted to emulate a smoother departure from the background. In the CPL calculation of the void Friedmann equation, we also found that [Goldberg and Vogeley \(2004\)](#)'s omission of a term that went unmentioned in their paper was a valid choice, as the difference was negligible over all times, provided that the initial choice of the scale factor obeyed $a_i \ll 1$ (see Figure 3.3).

While we successfully incorporated the CPL parametrization of the EoS into this model of a void, there were significant complications. For one, identical values of η_f , or the value of $\eta(t)$ at $z = 0$, led to massive discrepancies between the Λ CDM and CPL void scale factors. Additionally, we added a parameter t_{div} that signified the time at which the void detached from the global Hubble flow and began its separate evolution with a larger effective Hubble parameter than the background cosmology. This parameter reflected a huge difference between the two models as well. So while we expected there to be differences between the models when $w_0 \neq -1$ and $w_a \neq 0$, the secondary parameters of η_f and t_{div} having such a large impact on the void α made it very difficult to directly compare them.

However, these discrepancies did not render our CPL model useless. We took the model and applied it to a simplified version of void formation and expansion. In particular, the void size distribution derived from this step showed some useful behaviors that replicate what theory and observation tell us, namely that there is a characteristic void size at a given epoch. While we do not have enough information

from our model to definitively say that the void size distribution is a useful probe of dark energy, we know that voids are dominated by dark energy earlier than the background universe from Figure 3.5, and are therefore sensitive to dark energy and its EoS. However, Verza et al. (2019) used the double-barrier excursion set and Fisher-matrix approach, and found in halo catalogues from numerical simulations that voids and specifically the void distribution function are a good probes of the dark energy EoS. Therefore, this is and will continue to be a beneficial avenue of inquiry for cosmologists.

There are several things that future works can do to improve upon this analysis. Firstly, it would be best to apply our results to numerical simulations that account for the effects of the local environment, since we only considered isolated voids, which do not exist in the universe. Secondly, the effect of the void-in-cloud phenomenon needs to be accounted for using the double-barrier excursion set set forth in Sheth and van de Weygaert (2004) and subsequently improved on by Jennings et al. (2013). Using this approach to void formation and sociology also takes into account voids merging which our analysis omitted. Also, future work could improve on the modeling of the density profiles, so instead of treating it as a single parameter as we did, one could use work such as Hamaus et al. (2014) to get more realistic models of voids. Additionally, applying this work to simulations will not be enough. Next-generation surveys and observing tools such asWFIRST, DESI, the Nancy Grace Roman Telescope, and EUCLID will increase precision, volume, and statistics so that studying voids, and in particular large voids, will become increasingly useful in the study of dark energy. These surveys' larger redshift ranges will allow us to create better constraints on void abundance.

Bibliography

- Basilakos, S. and Nesseris, S. Conjoined constraints on modified gravity from the expansion history and cosmic growth. *Phys. Rev. D*, 96(6):063517, Sept. 2017. doi: 10.1103/PhysRevD.96.063517.
- Birkhoff, G. D. and Langer, R. E. *Relativity and modern physics*. 1923.
- Brunino, R., Trujillo, I., Pearce, F. R., and Thomas, P. A. The orientation of galaxy dark matter haloes around cosmic voids. *MNRAS*, 375(1):184–190, Feb. 2007. doi: 10.1111/j.1365-2966.2006.11282.x.
- Chevallier, M. and Polarski, D. Accelerating Universes with Scaling Dark Matter. *International Journal of Modern Physics D*, 10(2):213–223, Jan. 2001. doi: 10.1142/S0218271801000822.
- Clifton, T., Ferreira, P. G., Padilla, A., and Skordis, C. Modified gravity and cosmology. *Phys. Rep.*, 513(1):1–189, Mar. 2012. doi: 10.1016/j.physrep.2012.01.001.
- Colberg, J. M., Sheth, R. K., Diaferio, A., Gao, L., and Yoshida, N. Voids in a Λ CDM universe. *MNRAS*, 360(1):216–226, June 2005. doi: 10.1111/j.1365-2966.2005.09064.x.
- Colberg, J. M., Pearce, F., Foster, C., Platen, E., Brunino, R., Neyrinck, M., Basilakos, S., Fairall, A., Feldman, H., Gottlöber, S., Hahn, O., Hoyle, F., Müller, V., Nelson, L., Plionis, M., Porciani, C., Shandarin, S., Vogeley, M. S., and van de Weygaert, R. The Aspen-Amsterdam void finder comparison project. *MNRAS*, 387(2):933–944, June 2008. doi: 10.1111/j.1365-2966.2008.13307.x.
- Cole, S., Percival, W. J., Peacock, J. A., Norberg, P., Baugh, C. M., Frenk, C. S., Baldry, I., Bland-Hawthorn, J., Bridges, T., Cannon, R., Colless, M., Collins, C., Couch, W., Cross, N. J. G., Dalton, G., Eke, V. R., De Propris, R., Driver, S. P., Efstathiou, G., Ellis, R. S., Glazebrook, K., Jackson, C., Jenkins, A., Lahav, O., Lewis, I., Lumsden, S., Maddox, S., Madgwick, D., Peterson, B. A., Sutherland, W., and Taylor, K. The 2dF Galaxy Redshift Survey: power-spectrum analysis of the final data set and cosmological implications. *MNRAS*, 362(2):505–534, Sept. 2005. doi: 10.1111/j.1365-2966.2005.09318.x.
- Debono, I. and Smoot, G. F. General Relativity and Cosmology: Unsolved Questions and Future Directions. *Universe*, 2(4):23, Sept. 2016. doi: 10.3390/universe2040023.

- Einstein, A. Kosmologische Betrachtungen zur allgemeinen Relativitätstheorie. *Sitzungsberichte der Königlich Preußischen Akademie der Wissenschaften (Berlin)*, pages 142–152, Jan. 1917.
- El-Ad, H. and Piran, T. Voids in the Large-Scale Structure. *ApJ*, 491(2):421–435, Dec. 1997. doi: 10.1086/304973.
- Elyiv, A., Marulli, F., Pollina, G., Baldi, M., Branchini, E., Cimatti, A., and Moscardini, L. Cosmic voids detection without density measurements. *MNRAS*, 448(1):642–653, Mar. 2015. doi: 10.1093/mnras/stv043.
- Fabris, J. C., Goncalves, S. V. B., and de Souza, P. E. Fitting the Supernova Type Ia Data with the Chaplygin Gas. *arXiv e-prints*, art. astro-ph/0207430, July 2002.
- Goldberg, D. M. and Vogeley, M. S. Simulating Voids. *ApJ*, 605(1):1–6, Apr. 2004. doi: 10.1086/382143.
- Hamaus, N., Sutter, P. M., and Wandelt, B. D. Universal Density Profile for Cosmic Voids. *Phys. Rev. Lett.*, 112(25):251302, June 2014. doi: 10.1103/PhysRevLett.112.251302.
- Hausman, M. A., Olson, D. W., and Roth, B. D. The evolution of voids in the expanding universe. *ApJ*, 270:351–359, July 1983. doi: 10.1086/161128.
- Hoyle, F. and Vogeley, M. S. Voids in the Point Source Catalogue Survey and the Updated Zwicky Catalog. *ApJ*, 566(2):641–651, Feb. 2002. doi: 10.1086/338340.
- Hubble, E. A Relation between Distance and Radial Velocity among Extra-Galactic Nebulae. *Proceedings of the National Academy of Science*, 15(3):168–173, Mar. 1929. doi: 10.1073/pnas.15.3.168.
- Icke, V. Voids and filaments. *MNRAS*, 206:1P–3P, Jan. 1984. doi: 10.1093/mnras/206.1.1P.
- Jennings, E., Li, Y., and Hu, W. The abundance of voids and the excursion set formalism. *MNRAS*, 434(3):2167–2181, Sept. 2013. doi: 10.1093/mnras/stt1169.
- Khoury, J. and Weltman, A. Chameleon Fields: Awaiting Surprises for Tests of Gravity in Space. *Phys. Rev. Lett.*, 93(17):171104, Oct. 2004. doi: 10.1103/PhysRevLett.93.171104.
- Kitaura, F.-S., Chuang, C.-H., Liang, Y., Zhao, C., Tao, C., Rodríguez-Torres, S., Eisenstein, D. J., Gil-Marín, H., Kneib, J.-P., McBride, C., Percival, W. J., Ross, A. J., Sánchez, A. G., Tinker, J., Tojeiro, R., Vargas-Magana, M., and Zhao, G.-B. Signatures of the Primordial Universe from Its Emptiness: Measurement of Baryon Acoustic Oscillations from Minima of the Density Field. *Phys. Rev. Lett.*, 116(17):171301, Apr. 2016. doi: 10.1103/PhysRevLett.116.171301.

- Kreisch, C. D., Pisani, A., Carbone, C., Liu, J., Hawken, A. J., Massara, E., Spergel, D. N., and Wandelt, B. D. Massive neutrinos leave fingerprints on cosmic voids. *MNRAS*, 488(3):4413–4426, Sept. 2019. doi: 10.1093/mnras/stz1944.
- Lavaux, G. and Wandelt, B. D. Precision cosmology with voids: definition, methods, dynamics. *MNRAS*, 403(3):1392–1408, Apr. 2010. doi: 10.1111/j.1365-2966.2010.16197.x.
- Lavaux, G. and Wandelt, B. D. Precision Cosmography with Stacked Voids. *ApJ*, 754(2):109, Aug. 2012. doi: 10.1088/0004-637X/754/2/109.
- Leavitt, H. S. and Pickering, E. C. Periods of 25 Variable Stars in the Small Magellanic Cloud. *Harvard College Observatory Circular*, 173:1–3, Mar. 1912.
- Linder, E. V. Exploring the Expansion History of the Universe. *Phys. Rev. Lett.*, 90(9):091301, Mar. 2003. doi: 10.1103/PhysRevLett.90.091301.
- Mather, J. C., Cheng, E. S., Cottingham, D. A., Eplee, J. R. E., Fixsen, D. J., Hewagama, T., Isaacman, R. B., Jensen, K. A., Meyer, S. S., Noerdlinger, P. D., Read, S. M., Rosen, L. P., Shafer, R. A., Wright, E. L., Bennett, C. L., Boggess, N. W., Hauser, M. G., Kelsall, T., Moseley, J. S. H., Silverberg, R. F., Smoot, G. F., Weiss, R., and Wilkinson, D. T. Measurement of the Cosmic Microwave Background Spectrum by the COBE FIRAS Instrument. *ApJ*, 420:439, Jan. 1994. doi: 10.1086/173574.
- Micheletti, D., Iovino, A., Hawken, et al. The VIMOS Public Extragalactic Redshift Survey. Searching for cosmic voids. *A&A*, 570:A106, Oct. 2014. doi: 10.1051/0004-6361/201424107.
- Nadathur, S. and Hotchkiss, S. A robust public catalogue of voids and superclusters in the SDSS Data Release 7 galaxy surveys. *MNRAS*, 440(2):1248–1262, May 2014. doi: 10.1093/mnras/stu349.
- Neyrinck, M. C. ZOBOV: a parameter-free void-finding algorithm. *MNRAS*, 386(4):2101–2109, June 2008. doi: 10.1111/j.1365-2966.2008.13180.x.
- Neyrinck, M. C., Gnedin, N. Y., and Hamilton, A. J. S. VOBOZ: an almost-parameter-free halo-finding algorithm. *MNRAS*, 356(4):1222–1232, Feb. 2005. doi: 10.1111/j.1365-2966.2004.08505.x.
- Peebles, P. J. and Ratra, B. The cosmological constant and dark energy. *Reviews of Modern Physics*, 75(2):559–606, Apr. 2003. doi: 10.1103/RevModPhys.75.559.
- Penny, S. J., Brown, M. J. I., Pimbblet, K. A., et al. Galaxy And Mass Assembly (GAMA): the bright void galaxy population in the optical and mid-IR. *MNRAS*, 453(4):3519–3539, Nov. 2015. doi: 10.1093/mnras/stv1926.
- Perlmutter, S., Aldering, G., Goldhaber, G., et al. Measurements of Ω and Λ from 42 High-Redshift Supernovae. *ApJ*, 517(2):565–586, June 1999. doi: 10.1086/307221.

- Planck Collaboration, Ade, P. A. R., Aghanim, N., Arnaud, M., et al. Planck 2015 results. XIII. Cosmological parameters. *A&A*, 594:A13, Sept. 2016. doi: 10.1051/0004-6361/201525830.
- Planck Collaboration, Aghanim, N., Akrami, Y., Ashdown, M., et al. Planck 2018 results. VI. Cosmological parameters. *arXiv e-prints*, art. arXiv:1807.06209, July 2018.
- Platen, E., van de Weygaert, R., and Jones, B. J. T. A cosmic watershed: the WVF void detection technique. *MNRAS*, 380(2):551–570, Sept. 2007. doi: 10.1111/j.1365-2966.2007.12125.x.
- Platen, E., van de Weygaert, R., and Jones, B. J. T. Alignment of voids in the cosmic web. *MNRAS*, 387(1):128–136, June 2008. doi: 10.1111/j.1365-2966.2008.13019.x.
- Plionis, M. and Basilakos, S. The size and shape of local voids. *MNRAS*, 330(2):399–404, Feb. 2002. doi: 10.1046/j.1365-8711.2002.05069.x.
- Pycke, J. R. and Russell, E. A New Statistical Perspective on the Cosmic Void Distribution. *ApJ*, 821(2):110, Apr. 2016. doi: 10.3847/0004-637X/821/2/110.
- Ratra, B. and Peebles, P. J. E. Cosmological consequences of a rolling homogeneous scalar field. *Phys. Rev. D*, 37(12):3406–3427, June 1988. doi: 10.1103/PhysRevD.37.3406.
- Riess, A. G., Filippenko, A. V., Challis, P., Clocchiatti, A., Diercks, A., Garnavich, P. M., Gilliland, R. L., Hogan, C. J., Jha, S., Kirshner, R. P., Leibundgut, B., Phillips, M. M., Reiss, D., Schmidt, B. P., Schommer, R. A., Smith, R. C., Spyromilio, J., Stubbs, C., Suntzeff, N. B., and Tonry, J. Observational Evidence from Supernovae for an Accelerating Universe and a Cosmological Constant. *AJ*, 116(3):1009–1038, Sept. 1998. doi: 10.1086/300499.
- Riess, A. G., Macri, L. M., Hoffmann, S. L., Scolnic, D., Casertano, S., Filippenko, A. V., Tucker, B. E., Reid, M. J., Jones, D. O., Silverman, J. M., Chornock, R., Challis, P., Yuan, W., Brown, P. J., and Foley, R. J. A 2.4% Determination of the Local Value of the Hubble Constant. *ApJ*, 826(1):56, July 2016. doi: 10.3847/0004-637X/826/1/56.
- Sandage, A. and Tammann, G. A. Steps toward the Hubble constant. VIII - The global value. *ApJ*, 256:339–345, May 1982. doi: 10.1086/159911.
- Shandarin, S., Feldman, H. A., Heitmann, K., and Habib, S. Shapes and sizes of voids in the Lambda cold dark matter universe: excursion set approach. *MNRAS*, 367(4):1629–1640, Apr. 2006. doi: 10.1111/j.1365-2966.2006.10062.x.
- Sheth, R. K. and Tormen, G. An excursion set model of hierarchical clustering: ellipsoidal collapse and the moving barrier. *MNRAS*, 329(1):61–75, Jan. 2002. doi: 10.1046/j.1365-8711.2002.04950.x.

Sheth, R. K. and van de Weygaert, R. A hierarchy of voids: much ado about nothing. *MNRAS*, 350(2):517–538, May 2004. doi: 10.1111/j.1365-2966.2004.07661.x.

Slipher, V. M. Unusual Nebular Spectra. *PASP*, 30(178):346, Dec. 1918. doi: 10.1086/122775.

Spergel, D. N., Verde, L., Peiris, H. V., Komatsu, E., Nolta, M. R., Bennett, C. L., Halpern, M., Hinshaw, G., Jarosik, N., Kogut, A., Limon, M., Meyer, S. S., Page, L., Tucker, G. S., Weiland, J. L., Wollack, E., and Wright, E. L. First-Year Wilkinson Microwave Anisotropy Probe (WMAP) Observations: Determination of Cosmological Parameters. *ApJS*, 148(1):175–194, Sept. 2003. doi: 10.1086/377226.

Springel, V., White, S. D. M., Jenkins, A., Frenk, C. S., Yoshida, N., Gao, L., Navarro, J., Thacker, R., Croton, D., Helly, J., Peacock, J. A., Cole, S., Thomas, P., Couchman, H., Evrard, A., Colberg, J., and Pearce, F. Simulations of the formation, evolution and clustering of galaxies and quasars. *Nature*, 435(7042):629–636, June 2005. doi: 10.1038/nature03597.

Sutter, P. M., Lavaux, G., Wandelt, B. D., and Weinberg, D. H. A Public Void Catalog from the SDSS DR7 Galaxy Redshift Surveys Based on the Watershed Transform. *ApJ*, 761(1):44, Dec. 2012. doi: 10.1088/0004-637X/761/1/44.

Sutter, P. M., Lavaux, G., Hamaus, N., Pisani, A., Wandelt, B. D., Warren, M., Villaescusa-Navarro, F., Zivick, P., Mao, Q., and Thompson, B. B. VIDE: The Void IDentification and Examination toolkit. *Astronomy and Computing*, 9:1–9, Mar. 2015. doi: 10.1016/j.ascom.2014.10.002.

Szapudi, I., Kovács, A., Granett, B. R., Frei, Z., Silk, J., Garcia-Bellido, J., Burgett, W., Cole, S., Draper, P. W., Farrow, D. J., Kaiser, N., Magnier, E. A., Metcalfe, N., Morgan, J. S., Price, P., Tonry, J., and Wainscoat, R. The Cold Spot in the Cosmic Microwave Background: the Shadow of a Supervoid. *arXiv e-prints*, art. arXiv:1406.3622, June 2014.

Tikhonov, A. V. and Karachentsev, I. D. Minivoids in the Local Volume. *ApJ*, 653(2):969–976, Dec. 2006. doi: 10.1086/508981.

van de Weygaert, R. and Platen, E. Cosmic Voids: Structure, Dynamics and Galaxies. In *International Journal of Modern Physics Conference Series*, volume 1 of *International Journal of Modern Physics Conference Series*, pages 41–66, Jan. 2011. doi: 10.1142/S2010194511000092.

Verza, G., Pisani, A., Carbone, C., Hamaus, N., and Guzzo, L. The void size function in dynamical dark energy cosmologies. *J. Cosmology Astropart. Phys.*, 2019(12):040, Dec. 2019. doi: 10.1088/1475-7516/2019/12/040.

Weinberg, S. *Gravitation and Cosmology: Principles and Applications of the General Theory of Relativity*. 1972.

Weinberg, S. *Cosmology*. 2008.